S100A8-mediated metabolic adaptation controls HIV-1 persistence in macrophages in vivo

Fernando Real, Aiwei Zhu, Boxin Huang, Ania Belmellat, Alexis Sennepin, Thomas Vogl, Céline Ransy, Marc Revol, Riccardo Arrigucci, Anne Lombès, et al.

Peer Review Information: *Nature Communications* thanks Shokrollah Elahi, Neeltje Kootstra, and the other, anonymous, reviewer(s) for their contribution to the peer review of this work.

Title

S100A8-mediated metabolic adaptation controls HIV-1 persistence in macrophages *in vivo*

Author list

Fernando Real[1,2,3], Aiwei Zhu[1,2,3], Boxin Huang[1,2,3], Ania Belmellat[1,2,3], Alexis Sennepin[1,2,3], Thomas Vogl[4], Céline Ransy[2,3], Marc Revol[5], Riccardo Arrigucci[6], Anne Lombès[2,3], Johannes Roth[4], Maria Laura Gennaro[6], Frédéric Bouillaud[2,3], Sarra Cristofari[5], Morgane Bomsel[1,2,3*]

Affiliations

[1]Laboratory of Mucosal Entry of HIV and Mucosal Immunity, Institut Cochin, Université Paris Cité, 75014 Paris, France.

[2] CNRS, UMR8104, 75014 Paris, France.

[3] Inserm, U1016, Institut Cochin, 75014 Paris, France.

[4]Institute of Immunology and Interdisciplinary Center for Clinical Research, University of Münster, Münster, Germany.

[5]Plastic, Reconstructive and Aesthetic Surgery Department, Saint Louis Hospital, Paris, France.

[6]Public Health Research Institute, New Jersey Medical School, Rutgers, The State University of New Jersey, Newark, New Jersey, USA

*Corresponding author: morgane.bomsel@inserm.fr

Laboratory of Mucosal Entry of HIV and Mucosal Immunity, 3I Department, Cochin Institute, 75014 Paris, France

Telephone: +33-1-40-51-64-97

Fax: +33-1-40-51-64-54

Keywords: HIV-1, mucosa, tissue macrophage, S100A8, M4-macrophages, reservoir, glycolysis

Abstract

HIV-1 eradication is hindered by viral persistence in cell reservoirs, established not only in circulatory $CD4^+$T-cells but also in tissue-resident macrophages. The nature of macrophage reservoirs and mechanisms of persistence despite combined anti-retroviral therapy (cART) remain unclear. Using genital mucosa from cART-suppressed HIV-1-infected individuals, we evaluated the implication of macrophage immunometabolic pathways in HIV-1 persistence. We demonstrate that *ex-vivo*, macrophage tissue reservoirs contain transcriptionally active HIV-1 and viral particles accumulated in virus-containing compartments, and harbor an inflammatory IL-$1R^+$$S100A8^+$$MMP7^+$M4-phenotype prone to glycolysis. Reactivation of infectious virus production and release from these reservoirs *in-vitro* are induced by the alarmin S100A8, an endogenous factor produced by M4-macrophages and implicated in "sterile" inflammation. This process metabolically depends on glycolysis. Altogether, inflammatory M4-macrophages form a major tissue reservoir of replication-competent HIV-1, which reactivate viral production upon autocrine/paracrine S100A8-mediated glycolytic stimulation. This HIV-1 persistence pathway needs to be targeted in future HIV eradication strategies.

Introduction

Current HIV-1 combination antiretroviral therapy (cART) is neither curative nor eradicates infection largely due to the establishment of cell reservoirs for the virus, which persistently shelter HIV-1 through poorly understood mechanisms. Apart from classically described $CD4^+$ T-cell reservoirs, HIV-1 also establishes and persists in tissue macrophages [1, 2] by integrating viral genome [3] into macrophage DNA. Viral genome integration promotes viral replication for weeks post-infection with limited viral lytic egress [3, 4, 5], and finally resulting in latent macrophage infection [6].

The latency of macrophage infection, i.e. the reversibly nonproductive state of infection [7] in the weeks following infection has been demonstrated *in vitro* by restoring viral production of infected macrophage after activation of Toll-like receptor 4 (TLR4), the lipopolysaccharide (LPS) receptor [8] by LPS. Accordingly, LPS is known to reactivate, once silent, integrated proviral DNA [9, 10, 11]. In chronically or latently infected macrophages, TLR4 engagement induces a signal transduction pathway that culminates in the activation of the nuclear factor-kappa B (NF-κB) [11], which in turn efficiently triggers HIV-1 long-terminal repeat (LTR) promoters and HIV-1 replication [10].

There is growing evidence that macrophages are directly involved in the persistence of HIV-1 in tissues. [12, 13, 14], remaining transcriptionally active HIV-1 despite cART [7]. Similar to tissue-like macrophages infected *in vitro* [6], infected macrophages detected *in vivo* exhibit pathogen-containing vacuoles also known as virus-containing compartments (VCC). This structure is absent from infected $CD4^+$ T-cells that are unable to store viral particles. In macrophages, VCCs might serve as storage compartments for infectious virus produced despite cART and prone to be transferred to other target cells upon external stimulation

during cART [15] and/or once antiretroviral therapy is withdrawn [16]. We have previously shown that tissue-resident macrophages might constitute an important replication-competent HIV-1 reservoir [12]. This macrophage reservoir most likely forms during early tissue-macrophage infection during HIV-1 sexual transmission [6, 17]. *In vivo*, the degree of plasticity of macrophages is much higher than *in vitro*. Hence, the two main polarization states in which macrophage can be differentiated *in vitro* are the pro-inflammatory M1 and the pro-reparative M2 macrophage subtypes. In contrast *in vivo*, $CD68^{+}$ macrophages from HIV-1-infected cART-suppressed individuals harbor mainly a mixed M1/M2 phenotype expressing the IL-1 and IL-4 receptors, and CD206 but not the M2 marker CD163. As HIV chronic infection is associated to low-level chronic inflammation in the circulation but also in mucosal tissue, such mixed M1/M2 phenotype could correspond to the recently described inflammatory M4-macrophage subtype that contributes to atherosclerosis. This M4-macrophage subtype is characterized by expression of CD68, CD206, the metalloproteinase 7 (MMP7) and the calcium-binding protein A8 (S100A8) and which polarization is dependent on CXCL4/PF4 [18 19 20 21]. However, the precise characteristics of macrophage reservoirs at the single cell level, their capacity to remain transcriptionally active despite cART, and the mechanism supporting persistence of HIV-1 remain elusive.

HIV persistence mechanisms profoundly differ between T-cells and macrophages. In the later, it is tightly related to innate immunity inflammatory stimuli [22]. Furthermore, macrophages are key players in tissue homeostasis and reactive to metabolic adaptations potentially implicated in HIV-1 persistence [23, 24, 25]. We thus investigated whether mucosal macrophage HIV-1 reservoirs express inflammatory factors controlling reservoir maintenance, and whether in these reservoirs, macrophage metabolism could rule HIV-1 dynamics.

Here, we reveal that a specific macrophage subset, the inflammatory M4 one, is prone to glycolysis and constitute the principal viral mucosal reservoir. When facing an inflammatory stimulus such as that induced by the inflammatory alarmin S100 calcium binding protein A8 (S100A8) expressed in particular by tissue M4-macrophages and which can target TLR-4, the M4-macrophage metabolic profile shifts towards glycolysis. Furthermore, S100A8 maintains M4-macrophage reservoir persistence in an autocrine/paracrine loop and reactivates the production of replication-competent viral particles in male genital tract macrophages obtained from cART-suppressed individuals in a process controlled by a glycolytic metabolism adaptation.

The characterization of inflammatory M4-macrophages as the major HIV-1 reservoir in the genital mucosa from cART-suppressed individuals, together with the demonstration that macrophage glycolytic immuno-metabolism participates in HIV-1 latency reversal by controlling the production of infectious HIV-1 from these reservoirs, contribute to define novel pharmacological targets for a functional HIV-1 cure.

Results

Inflammatory macrophages with an M4 (S100A8$^+$MMP-7$^+$) phenotype are enriched in the genital mucosa of cART-suppressed HIV-1 infected-individuals

We previously identified the TLR-4 ligand LPS as an agent capable of reactivating replication competent HIV-1 from genital tissue suspension. This indicated that tissue macrophages might form major replication-competent HIV-1 reservoirs in these mucosa [6, 12], although the precise identity of these reservoirs remained unclear. We have assessed mucosal macrophages from urethral tissue from healthy and HIV-infected cART-treated individuals (Table 1) by a series of experiments using various techniques as summarized in Figure 1a. First, to determine the distinctive phenotype of HIV-1 reservoirs formed in tissue-resident macrophages at the single-cell level, we profiled the cytokines implicated in the polarization of different macrophage subtypes [26, 27] in urethral tissue lysate samples from healthy donors and cART-suppressed HIV-1 infected individuals comparatively, using the Luminex technology. C-X-C motif chemokine 4/ Platelet Factor 4 (CXCL4/PF4), Interleukin-13 (IL-13), Interferon-γ and Granulocyte-macrophage colony-stimulating factor (GM-CSF) were upregulated in mucosal tissue from cART-suppressed HIV-infected individuals as compared with non-infected donors (Figure 1b and Supplementary Figure 1a). CXCL4/PF4 directly correlated with IL-13 independently of the HIV status. However, only in the cART HIV$^+$ group, CXCL4/PF4 correlated directly with IFN-γ and inversely with IL-4 (Supplementary Figure 1b). The upregulation of CXCL4/PF4 in cART-suppressed HIV-infected individuals compared with healthy donors was confirmed by immunohistochemistry (Supplementary Figure 2).

IL-13 is implicated in the alternative activation of macrophages resulting in a pro-reparative CD206$^+$CD163$^+$ macrophage subset that antagonizes IFN-γ inflammatory actions and is implicated in humoral immunity, allergies and anti-parasitic responses [28]. The participation of *bona fide* pro-reparative CD163$^+$ macrophages to HIV-1 tissue reservoirs could be discarded based on our recent results showing that CD163^{neg} but CD206$^+$IL4-R$^+$IL1-R$^+$ macrophages with an intermediate pro-inflammatory/pro-reparative profile are enriched in urethral tissue of cART-treated patients [12], and are the likely site of HIV persistence in the male genital mucosa. However, IL-13 can also drive macrophage expression of DC-SIGN, an alternative receptor for HIV-1, thus rendering macrophages highly susceptible to HIV infection. The upregulation of IL-13 in mucosal tissues from cART-suppressed HIV-1-infected patients we observed might result from the immunomodulatory activity of CXCL4/PF4 on Th2 lymphocytes [29].

Furthermore, CXCL4/PF4 is mainly expressed by cells of the megakaryocyte lineage and consequently in platelets but also by some epithelial cells [26, 30]. One function of CXCL4/PF4 is to induce *in vitro* the polarization of macrophages toward the recently described M4 subset [31], an inflammatory macrophage subset related to foam cell formation, atherosclerosis and intracellular infection [26, 30]. M4-macrophages express inflammatory surface markers such as HLA-DR and CD86 but lack CD163 [26]. Such macrophage profile matches that of CD163^{neg} but CD206$^+$IL4-R$^+$IL1-R$^+$ activated macrophage subtype we have found implicated in mucosal persistence of HIV-1[12]. M4-macrophages are defined, both *in vitro* and *in vivo*, by the co-expression of the S100 calcium binding proteins (S100) A8 and S100A9 also known as

Myeloid-related protein 8 and 14 (MRP8 and MRP14) or Calgranulin A [30, 32], along with metalloproteinase 7 (MMP-7) [33]. The markers $CD68^{+}S100A8^{+}MMP\text{-}7^{+}$ thus identify M4-macrophages.

To search for M4-macrophage in urethral tissues in HIV/AIDS, we analyzed the frequency of total mucosal ($CD68^{+}$) macrophages in urethral cell suspensions and therein, the frequency of M4-macrophages ($S100A8^{+}MMP\text{-}7^{+}$) by flow cytometry (Figure 1c-d and Supplementary Figure 3). Although the frequency of macrophages did not differ between healthy donors and cART-suppressed HIV-infected individuals, M4-macrophages were enriched in urethral tissues from the HIV-1 infected group compared with healthy donors (Figure 1c-d). The expression of common markers of macrophage polarization in total urethral macrophages ($CD68^{+}$) as well as in M4-macrophages was also investigated. We observed an increased frequency of macrophages expressing the inflammatory markers CD86 and IL-1R among both total macrophages (Figure 1e left for frequencies and Supplementary Figure 3d left for MFI) and M4-macrophages (Figure 1e right for frequencies and Supplementary Figure 3d right for MFI) from cART-suppressed HIV-1 infected individuals compared with healthy donors.

Inflammatory $IL\text{-}1R^{+}$ M4-macrophages are the main HIV-1 mucosal macrophage reservoirs *in vivo*

The macrophage HIV reservoirs found in the urethral mucosal stroma from cART-suppressed individuals are a transcriptionally active reservoir in which HIV RNA was detected by fluorescent *in situ* hybridization (FISH) (Figure 2a). We quantified HIV-1-infected macrophages in urethral tissues from cART-suppressed individuals at the single-cell level combining FISH and flow cytometry referred to as FISH-flow [34, 35] to detect cell-associated HIV together with markers of different macrophage profiles, including the M4-defining S100A8 and MMP-7. We first validated the FISH-flow HIV-1 RNA probes using OM-10.1 cell lines (Supplementary Figure 4a-b) which constitutively harbor integrated HIV provirus and can be stimulated to produce more HIV-1 upon TNF-α stimulation [36].

In HIV-1-infected individuals despite cART-suppression, we detected a subpopulation of macrophages containing HIV-1 RNA and the viral capsid protein p24 (Gag) that represents 0.3% [CI: 0.12-0.48] of total mucosal macrophages present in tissue cell suspensions (Figure 2b-c and Supplementary Figure 4c).

To characterize these HIV^{+} macrophages, we generated UMAPs from the multiparametric flow cytometry analysis including S100A8, MMP-7, IL-1R, IL-4R, CD206 and CD163 markers and compiling data from 4 cART HIV^{+} individuals. The rare HIV^{+} macrophages detected were backgated into this UMAP (Figure 2d). The results showed that HIV^{+} macrophages were distributed in the M4 population (light blue population in UMAP, $S100A8^{+}MMP\text{-}7^{+}CD206^{+}IL\text{-}1R^{+}$) and in a second population (purple population in UMAP) characterized by $S100A8^{neg}MMP\text{-}7^{+}CD206^{+}IL\text{-}1R^{+}$ macrophages. Around half of the infected macrophages (52.7 % [CI: 16.6-100]) belonged to the $S100A8^{+}MMP\text{-}7^{+}$ M4-macrophage profile (Supplementary Figure 4d). Furthermore, these HIV-1-infected macrophages expressed also CD206, IL-4R and IL-1R but not CD163 (Figure 2d and Supplementary Figure 3d), in agreement with the previously

uncharacterized CD206^{+}IL4-R^{+}IL1-R^{+}CD163^{neg} intermediary subset (Mi) of macrophages we found enriched in the male urethra of cART-suppressed individuals [12]. Finally, S100A8 was expressed by the macrophage HIV reservoirs as demonstrated by the immunodetection of S100A8 within HIV-1 reservoirs identified as CD68^{+}/HIV-1 RNA^{+} cells using combined immunohistochemistry and RNAscope FISH (Figure 2e).

Altogether, we have identified a transcriptionally active (HIV-1 RNA^{+}) reservoir formed mainly in M4-macrophages that express the pro-inflammatory activation marker IL-1R and, importantly, the alarmin S100A8.

In vitro derived and latently infected M4-macrophages are surrogates of HIV-1 mucosal macrophage reservoirs

As mucosal tissues from HIV-1 infected individuals are rare, hampering the characterization of HIV reservoir dynamic, we established alternative models of HIV-1 reservoir in macrophages, either from monocytes or from tissue macrophages infected *in vitro* until latency self-establishment.

M4-macrophages can be differentiated from blood monocytes *in vitro* by culture in the presence of CXCL4/PF4 [30, 32], resulting in M4-monocytes derived macrophages (MDM). We first investigated whether M4-MDM would be surrogates of the tissue macrophages found in the urethral mucosa by flow cytometry. Relative to the expression of tested macrophage surface markers, especially S100A8, one subunit of the heterodimeric S100A8/S100A9 complex, we found that M4-MDM were more closely related to the population of urethral macrophages isolated either from HIV-1-infected or healthy individuals than other *in vitro* derived macrophage subtypes, namely "classically" activated pro-inflammatory M1-MDM (induced by GM-CSF, IFN-γ and LPS) and alternatively activated pro-reparative M2-MDM (induced by M-CSF, IL-4 and IL-13) (Figure 3a).

When infected with HIV-1, the different MDM subsets were productively infected. At later time points, whereas non-polarized-MDM induced by GM-CSF/M-CSF or M2-MDM, although at a lower level in agreement with others [3, 24], continue both to produce viral particles until day 49 after infection as detected by p24 ELISA, M4-MDM reduced viral production and enters latency characterized by undetectable viral production from day 8.5 [CI: 7-15] (Figure 3b).

At the morphological level, M4-MDM harbored viruses in virus-containing compartments (VCCs) (Figure 3c) during the latent phase of viral production, i.e., when macrophages stop producing new viral particles into the culture medium. Similarly, in mucosal tissues CD68^{+} macrophages sheltered HIV-1 in VCCs as detected by p24 labeling (Figure 3d). We next performed morphometric analyses of VCCs formed *in vitro* by latently infected M4-MDM (Figure 3e) and formed *in vivo* by mucosal macrophages in tissues (Figure 3f). These analyses revealed that although VCCs in M4-MDM were more heterogeneous in size, number and scattering, the sum of the VCCs volume per infected macrophage did not differ from that in

infected mucosal tissue macrophage reservoirs formed *in vivo*. A panel of additional macrophage VCCs detected *in vivo* in tissues is shown in Supplementary Figure 5a.

Finally, we also infected genuine mucosal tissue macrophages purified from healthy donor tissue by HIV-1 *in vitro*. Tissue macrophages were productively infected by HIV-1 in a similar manner to M4-MDM, but established latency even earlier, reaching latency after a median interval of 5 [CI: 3-10] days post-infection (Figure 3g) compared with 8.5 [CI: 7-15] days post-infection for M4-MDM. Viral production by *ex vivo*-infected urethral macrophages is abrogated by the antiretroviral drug Zidovudine (AZT), confirming productive infection (Figure 3h).

We thus established two reliable surrogates of the tissue macrophage reservoirs found in urethral mucosa, formed by M4-MDM and tissue macrophages acutely infected *in vitro* by HIV-1 and maintained at least for a week in culture.

S100A8 can reactivate the production of replication-competent virus from macrophage reservoirs

S100A8 is always expressed together with S100A9 as a heterodimer [37]. However, to show the full activity of the S100A8/S100A9 complex, it is necessary to use S100A8 homodimers in cell culture studies because the activity of the heterodimer is very low *in vitro* due to the formation of heterotetramers that blocks the S100A8/S100A9 complex activity [37].

S100A8/S100A9 activates specifically TLR4 [38], which in turn can reactivate HIV-1 production [39]. We thus hypothesized that formation and persistence of HIV-1 reservoirs in M4-macrophages is regulated by a local S100A8/S100A9-mediated low-level HIV-1 production in genital tissues. When secreted in tissues, mainly from neutrophils or macrophages, S100A8/S100A9 forms rapidly heterotetramers [37], thereby buffering its activity. It might remain nevertheless a short window of time during which the S100A8/S100A9 heterodimer could be active locally in an autocrine/paracrine fashion.

We thus measured the levels of S100A8 monomer and S100A8/S100A9 heterodimers in urethral tissues by ELISA. S100A8/S100A9 heterodimer, the physiologically relevant form, was expressed at much higher concentration than the S100A8 monomer, as expected. Furthermore, the S100A8/S100A9 heterodimer concentration was significantly reduced in cART-suppressed HIV-1-infected individual as compared with healthy donor tissues (Figure 4a), in line with increased neutrophil cell death observed in HIV-infected individuals on cART [40].

We further investigated whether the measured tissue S100A8 and its expression at the tissue macrophage level were associated. When analyzed by flow cytometry, the frequency of $S100A8^{+}$ cells remained similar in both healthy donors and HIV-1-infected individuals. However, the expression of S100A8 per cell, corresponding to the MFI, was specifically upregulated in M4-macrophages isolated from cART-suppressed HIV-1-infected individuals compared with tissue M4-macrophages from non-infected individuals but also with cells from the entire tissue cell population and total tissue macrophage population of infected and non-infected individuals (Figure 4b). Therefore, although the total mucosal tissue

S100A8/S100A9 heterodimer level was decreased in cART-suppressed infected individuals, the level of S100A8 was higher in M4-macrophages from cART-suppressed infected individuals, the main macrophage subset that host HIV-1, compared with healthy donor ones. In tissue from cART- treated individuals that are subjected to chronic low-level inflammation [41], S100A8 could be locally secreted upon M4-macrophage stimulation and act in an autocrine/paracrine manner to reactivate the macrophage reservoirs upon binding to TLR4.

To investigate the capacity of S100A8 to reverse HIV-1 latency in macrophage reservoirs, we first evaluated whether S100A8 treatment would reverse latency in HIV-1-infected M4-MDM. For these cell culture-based studies, we used the homodimer S100A8 instead of the physiological relevant heterocomplex S100A8/S100A9 due to the rapid loss of activity by heterotetramerization [37]. S100A8 resumed viral production from a HIV-1 latent state in M4-MDM (Figure 4c) in a concentration-dependent manner from 5 to 20µg/ml, as measured by p24 ELISA. Latency reversal by S100A8 was as efficient as that induced by LPS at a concentration of 1 µg/ml, a treatment we and others have already shown to reactivate HIV-1 production from macrophages latently infected by HIV *in vitro* or *in vivo* [6, 12]. Moreover, in latently infected M4-MDM, HIV DNA was found integrated in the host cell genome, as measured by Alu-gag nested PCR (Supplementary Figure 5b, left). Addition of S100A8 to latently infected M4-macrophages resumed viral transcription. S100A8-mediated viral reactivation is specific, as the antiretroviral drug AZT blocked it to level prior to reactivation (Supplementary Figure 5b, right).

Furthermore, S100A8 at 10µg/ml was also efficient at reactivating viral production from mucosal tissue macrophages isolated from healthy donors and latently infected by HIV-1 *in vitro* used as another HIV-1 macrophage reservoir surrogate (Figure 4d).

Finally, S100A8 reversed latency in tissue macrophages isolated from cART-suppressed HIV-1-infected individuals. The reactivated virus was replication-competent as quantified in a viral outgrowth assay using activated $CD4^+$ T-cells (Figure 4e). Additionally in tissues from cART-treated individuals, HIV-1 RNA *in situ* hybridization coupled to p24-Gag immunodetection in $CD68^+$ macrophages further demonstrated that clusters of p24 (Gag) proteins co-localized with HIV-1 RNA, a pattern suggestive of VCCs before *ex vivo* S100A8 treatment (Supplementary Figure 5c upper). Upon S100A8-mediated HIV-1 reactivation, both HIV-1 RNA and protein relocalized at the macrophage plasma membrane that is suggestive of extemporaneous production of new HIV-1 particles and/or mobilization of VCCs to the macrophage plasma membrane in the process of releasing their virus content (Supplementary Figure 5c lower).

S100A8-mediated reactivation of HIV-1 release from macrophage reservoirs depends on glycolysis

After engaging TLR4, microbial components such as LPS trigger a pro-inflammatory response in macrophages that was recently described to engage a metabolic reprogramming, which contributes to macrophage plasticity and physiology [42]. As we have shown that mucosal macrophage HIV-1 reservoirs

express pro-inflammatory markers (Figures 1 and 2), we investigated whether S100A8-mediated reactivation of the mucosal macrophage reservoirs would trigger a similar metabolic reprogramming related to inflammatory responses.

The macrophage metabolic profile varies according to macrophage polarization from pro-reparative to pro-inflammatory macrophages. In "classically" IFN-γ/LPS activated M1-macrophages, aerobic glycolysis is induced, as well as a glucose-induced repression of respiration, beneficial for aerobic glycolysis what is known as the Warburg effect in cancer cells [43]. "Alternative" IL-4/IL-13-activated M2-macrophages obtain energy preferentially from fatty acid oxidation and oxidative metabolism via oxidative phosphorylation (OXPHOS) [42]. Little is known about the metabolism of other alternative macrophage subsets implicated in inflammatory diseases such as the M4 subset [44]. We thus first investigated the metabolic profile of *in vitro*-derived inflammatory M4-macrophages compared with pro-reparative M2-macrophages. Therefore, M2- and M4-MDM basal metabolism was evaluated comparatively by measuring extracellular acidification rate (ECAR, to assess glycolysis) and oxygen consumption rate (OCR, to assess OXPHOS) upon injection of glucose into macrophage cultures. As a result, M4-MDM presented a mixed metabolic profile, carrying out glycolysis (inhibited by 2-deoxyglucose, or 2-DG) but also fatty acid oxidation (inhibited by etomoxir). Upon glucose addition to culture medium, M4-MDM glycolytic activity was higher than that of M2-MDM (Figure 5a left) whereas M4-MDM OCR was only slightly repressed compared to that of M2-MDM (Figure 5a right). By adding metabolic inhibitors to macrophages during their metabolic evaluation, the glycolytic activity of these cells could be recorded. As a result, M4-macrophages had a higher glycolytic activity than M2 macrophages (Figure 5b). As compared with M2-MDM which glycolytic activity remains close that of baseline after glucose addition, M4 were more prone for glycolysis. Indeed, after addition of glucose, M4-MDM glycolysis activity increased by 25% from baseline (Supplementary Figure 6a). These data define M4-macrophages as a pro-inflammatory, glycolytic subset among the spectrum of different macrophage immunometabolic profile.

Next, we evaluated the metabolic responses of M4-macrophages in glucose-supplemented medium after injection of medium alone (untreated), S100A8 (that we have shown above to act as HIV-1 latency reversal agent) or LPS. S100A8 triggered a significant glycolytic activity of M4-MDM, higher than that in the absence of stimulation, but less intense than the LPS-stimulated glycolysis (Figure 5c left and Fig. 5d). We observed an increase in glycolysis activity of ∼15%, ∼40% and ∼60% from baseline after injection of medium alone (untreated), S100A8 and LPS, respectively (Supplementary Figure 6b).

In contrast, S100A8 did not affect the OCR whereas LPS slightly decreased it (Figure 5c right) Altogether, LPS and S100A8 affected M4-macrophages metabolism by increasing mainly glycolysis with no major impact on cell mitochondrial respiration. These differences in the intensity of glycolytic activity in M4-macrophage upon stimulation by S100A8 and LPS may explain the difference in the intensity of latency reversal observed in M4-macrophage reservoirs treated with these two compounds

We next evaluated whether latency reversal in HIV-1 macrophage reservoirs can be triggered upon glycolytic stimulation via TLR4. Therefore, *in vivo* established tissue macrophage reservoirs obtained from

cART-suppressed HIV-1-infected individuals were treated with S100A8 to resume the production of replication-competent HIV-1 in the absence of or with pretreatment with the glycolytic inhibitor 2-DG as schematized in Figure 5e. S100A8 triggered HIV latency reversal in tissue macrophage reservoirs resulting in infectious virus production in the culture medium, as quantified in the outgrowth assays using $CD4^+$T-cells as reporter cells (Figure 5f). Inhibition of glycolysis before induction of latency reversal by S100A8 fully blocked the reactivation of replication-competent viral production by macrophages (Figure 5f). Altogether, immunometabolic glycolytic pathways control HIV-1 reservoir reactivation in tissue macrophages.

Discussion

The characterization of the degree of differentiation/polarization toward a specific macrophage subtype capable of hosting HIV-1 in human mucosal tissues permits to identify a central host cell therapeutic target for the virus in male genital mucosa. Macrophages are known to be extremely versatile cells, able to respond to a plethora of factors by differentiating into functionally distinct subsets. Each issue-specific environment, presenting a characteristic set of cytokines, could drive macrophages towards a HIV-1-resistant or -susceptible state, not necessarily associated to the *in vitro* established M1/M2 macrophage polarization paradigm [3, 27]. Our study is the first, to our knowledge, to measure macrophage-related cytokines in the urethral mucosa comparing healthy donors and HIV-infected individuals under cART. Despite effective blood viral suppression by cART, HIV-infected individuals present persistent chronic immune activation, albeit at low levels in blood and tissues [41, 45, 46]. Resulting change in microenvironment could polarize macrophages toward specialized profiles implicated in viral persistence.

Here, we demonstrated that in the urethral tissue from cART-suppressed HIV-infected patients, the HIV-1 replication-competent reservoir resides in a recently described subtype of inflammatory macrophages classified as M4. M4 polarization is mainly induced by CXCL4/PF4 [18, 19, 20, 21] that we have found upregulated in the urethral mucosa of cART-suppressed HIV^+ individuals as compared with healthy donors. Macrophages in most tissues are derived from embryonic progenitors, displaying long life span and self-renewal capacities, and blood monocytes contribute only minimally to the pool of tissue macrophages under homeostatic conditions [47]. However additionally, persistent tissue inflammation as commonly observed in HIV infection [48] might also contribute to reservoir establishment and persistence. Such persistent tissue inflammation would favor the entry and integration of monocytes in the resident macrophage pool in tissues [47], likely impacting viral reservoirs dynamics. Stable tissue HIV reservoirs would persist long-lived tissue macrophages, likely formed upon their early infection during sexual transmission [6, 17]. In addition, inflammatory macrophages-derived from blood monocytes [47] might also either replenish the macrophage reservoir by becoming infected or stimulate the production of viruses sheltered by latently infected macrophages once monocytes enter tissues. Furthermore, such monocyte-derived macrophages repopulating tissues and acquiring self-renewal capacities [47] could in turn be infected and become HIV reservoirs locally.

This could explain how the latently infected pool of macrophages in mucosal tissues is long-lasting and persists despite cART.

In this latter context, the production of endogenous inflammatory factors by monocytes such as alarmins can engage TLR and participate in endogenous "sterile" inflammation processes [37]. This would in turn promote a local tissue autocrine feedback loop favoring low-level of NF-kB-mediated HIV production despite systemic viral suppression. Such scenario is in agreement with the presence of whole viral particles in VCCs that we observed *in vivo* in reservoir macrophages in cART-suppressed patient tissues [12]. Unlike T cells, macrophages produce viral particles that mainly bud into and are stored in VCCs [16]. VCCs may thus contain incoming as well as *de novo* produced viruses. In the present model, latently infected M4-macrophages containing VCCs stop producing p24 to the extracellular milieu several days p.i.. suggesting that the source of virus detected in VCCs is likely not recently endocytosed virus. However, during the phase of active production of virions by infected macrophages, viruses could not only bud into VCCs [16], but could be also endocytosed and stored in VCCs, a feature requiring further investigations for which the M4 model is particularly useful.

The presence of virus in VCCs we observed further indicates that these infected tissue macrophages form a low-level productive reservoir, as suggested by others [49]. Maintenance of such low-level replication HIV-1 reservoirs, i.e., with sustained low-level viral production despite successful antiretroviral therapy, would involve a perennial inflammatory stimulus such as those observed in non-resolving inflammation, a chronic condition regulated by macrophages [50, 51].

Produced largely by neutrophils and macrophages, S100A8 forms a heterodimer with the S100 calcium binding protein A9 (S100A9 or MRP14), and this S100A8/S100A9 complex functions as pro-inflammatory damage-associated molecular patterns (DAMP) [37, 38, 52]. S100A8 is however the functional unit of the heterodimer able to engage TLR4 [38] that in turn activates NF-κB [53]. This mechanism of action converges with HIV-1 reactivation: indeed, S100A8 activates HIV-1 transcription in latently infected macrophages [54] and in $CD4^+$ T lymphocytes via the NF-κB axis [39]. Therefore, S100A8 could act as the exogenous bacterial component LPS by activating TLR-4 signaling, although less strongly and without affecting the cell oxygen consumption and mitochondrial respiration. S100A8 might thus be an inflammatory endogenous tissue factor able to stimulate the viral reservoir formed in latently infected macrophages to resume viral production.

Of note, S100A8 systemic levels are increased in HIV-1 patients as well as in other inflammatory diseases and viral infections [38, 54, 55, 56]. Furthermore, S100A8 levels rise also in genital mucosal secretions from HIV-1 infected patients where it can reactivate HIV-1 replication in latently infected cells [54]. However, in the context of antiretroviral therapy, we found that total S100A8 measured as heterodimer with S100A9 is down regulated in the urethral mucosa of cART-suppressed HIV-1-infected individuals compared with healthy donors. This decrease could be due to a decrease in the mucosa of cART-treated HIV-infected individuals in the frequency of tissue neutrophils that is the most abundant source of S100A8/S100A9 in tissues [38]. Therefore, the specific up-regulation of this alarmin in M4-macrophages we observed in cART-

suppressed HIV-1-infected individuals compared with healthy donors indicates that S100A8-induced HIV-1 reactivation in macrophage reservoirs likely occurs at a local level under mechanisms remaining to be elucidated. One can propose that S100A8, produced locally by M4-macrophages in a short time window prior the formation of heterotetramers with S100A9, binds immediately after secretion and in an autocrine/paracrine manner to TLR-4 at the M4-macrophage reservoir surface. This interaction would secure a regulatory mechanism for controlling the conversion from HIV-1 deep latency observed in $CD4^+$ T-cells [57] toward HIV active transcription and storage of virions in VCCs [12, 16] that we describe here.

One of the mechanisms regulating HIV-1 latency could be a metabolic reprogramming, a process central in macrophage pro-reparative/pro-inflammatory plasticity and in response to pathogens [58, 59]. Upon pattern recognition receptors (PRR) that engage DAMPs like S100A8 or pathogen-associated molecular patterns (PAMP) like LPS, macrophages rewire their transcriptional program to produce inflammatory factors and metabolic mediators responsible for the modification of macrophage metabolism for aerobic glycolysis, simultaneously [59]. LPS and S100A8 reverse HIV-1 latency in mucosal macrophage reservoirs, both factors inducing an inflammatory reaction and a glycolytic activity. This property could be used for the elimination of HIV-1 reservoirs [60]. Drugs could be developed to target the glycolytic metabolic pathways, offering an alternative, yet unexplored, for shock-and-kill or block-and-lock strategies. The advantage of such an approach is that macrophages can be "trained" upon recognition of inflammatory stimuli, rewiring their metabolism for days or months, as described in other infectious diseases [61]. Such long-lasting glycolytic stimulus would keep macrophage reservoirs producing virus until their recognition and elimination by $CD8^+$ cytotoxic T lymphocytes (CTL)-mediated killing, to which macrophages are resistant when acutely infected [62]. Pharmacological inhibition of glycolysis is known to profoundly interfere with the physiology of HIV-1 latently infected cells and HIV-1 reactivation [24, 25]. Therefore, a prolonged shift in glycolytic pathways towards different metabolic profiles could prevent macrophage reservoirs from producing viruses, in turn blocking a potential low-level replication of persistent HIV-1 in tissues.

Such blockade of glycolysis could also be exploited to eliminate the HIV-1 reservoir in $CD4^+$T-cells. Indeed, a glycolytic environment is required to carry out HIV-1 reverse transcription, and inhibition of glycolysis blocks HIV-1 replication, as recently demonstrated [25]. Altogether, the metabolism of cells targeted by HIV-1, either $CD4^+$T-cells or macrophages, emerges as an important common determinant of HIV-1 infection, even if regulated by different mechanisms.

Overall, our results reveal that a specific macrophage subset, the inflammatory M4 one, forms viral mucosal HIV-1 reservoir and promotes viral persistence that is regulated by the endogenously expressed S100A8, which would mediate sustained low-level HIV-1 production in the male genital tract. Such novel HIV-1 reservoir in M4-macrophages adds to the blood T-cell reservoir and now needs also to be targeted by eradication strategies. The requirement for glycolysis in HIV-1 reservoir reactivation reveals a stage of vulnerability that can be exploited in future HIV-1 cure strategies.

Methods

Ethical statement. The study was conducted under local ethical regulation after approval by the local ethical committee (Comité de Protection des Personnes, Île de France XI; approval number 11 016). Human samples were obtained after written informed consent from all study participants.

Urethral mucosa tissue cell suspensions and sorting of monocytic/macrophagic urethral cells. Penile tissues were obtained from individuals undergoing elective gender reassignment surgery at the Saint Louis Hospital in Paris, France. These included healthy individuals and also HIV-infected ones (median age of 43 years old [CI: 37-49], infected with HIV-1 for a median duration of 11.5 years [CI: 4-17]) under suppressive cART for a median period of 9.5 years [4-12.9] with undetectable plasma viral loads (<40 RNA copies/ml) for at least 12 months before surgery (Table 1). Immediately following surgery, the penile tissues were preserved in phosphate-buffered saline (PBS) supplemented with 100 U/ml penicillin and 100 µg/ml streptomycin (Gibco, ThermoFisher Scientific) and transported on ice to a biosecurity level 2+ facility. Tissues were processed to obtain a tissue cell suspension of urethral mucosal cells as described [17]. Viability of tissue macrophages after tissue processing was evaluated by DRAQ7 staining (BD biosciences) following manufacturer instructions, before and after removal of dead cells by magnetic isolation (dead cell removal kit, Miltenyi Biotec GmbH). Accordingly, viable macrophages corresponded to >90% (before) and >95% (after dead cell removal) of cells among the population of total tissue macrophages ($CD68^+$) in the cell suspension (Supplementary Figure 3a).

The $CD14^+CD16^+$ cell population was sorted from total tissue cell suspensions using magnetic microbeads (Miltenyi Biotec GmbH) following manufacturer instruction. A mean percentage of 58% [CI: 49.12-66.8] cells in the $CD14^+CD16^+$ selected urethral mucosal cell population corresponds to $CD68^+$ macrophages with less than 1% corresponding to $CD3^+$ T-cells, as quantified by flow cytometry. Potential $CD3^+$ cell contaminants were thoroughly washed out from the plates before *ex vivo* macrophage cultivation, infection and latency reversal experiments.

Ex vivo *cultivation of urethral macrophages.* The total $CD14^+CD16^+$ urethral mucosal cell population was cultivated in flat-bottom well plates ($5x10^3$ cells per mm^2 of well area) to which mainly macrophages remained attached after overnight incubation at 37°C 5% CO_2 and non-adherent or less adherent cells were thoroughly washed out. The remaining attached tissue macrophages were then cultivated in RPMI 1640 culture medium supplemented with 10% fetal calf serum (FCS) and employed for *in vitro* HIV infection or HIV latency reversal assays.

Monocyte isolation and macrophage culture. $CD14^+$ cells (monocytes) peripheral blood mononuclear cells (PBMCs) obtained by negative selection (STEMCELL Technologies Inc.) according to manufacturer instruction were differentiated *in vitro* into macrophages. Monocyte derived macrophage (MDM) subtypes were obtained using the following regimens in RPMI 1640 with 10% FCS: i) for M1-macrophages: 6 days

of 50 ng/ml granulocyte-macrophage colony-stimulating factor (GM-CSF, R&D Systems) followed by 20 ng/ml interferon gamma (IFN-γ, R&D Systems) and 1 μg/ml lipopolysaccharide (LPS from *Salmonella enterica* serotype typhimurium, Sigma-Aldrich) for additional 2 days; ii) for M2a-macrophages: 6 days of 25 ng/ml macrophage colony-stimulating factor (M-CSF, R&D Systems) followed by 20 ng/ml interleukin 4 (IL-4, R&D Systems) and 20 ng/ml IL-13 (R&D Systems) cytokines for additional 2 days [63]; or 3 iii) for M4-macrophages: 30 μg/ml C-X-C motif chemokine 4/Platelet Factor 4 cytokine (CXCL4/PF4, Chromatec GmbH) for 6 days [26, 31]. Non-polarized MDM were produced by cultivation in complete medium supplemented with 50 ng/ml GM-CSF and 25 ng/ml M-CSF for 6 days.

In vitro *and* ex vivo *HIV infection.* *In vitro* and *ex vivo* infection experiments were performed using MDM from healthy donors or urethral tissue macrophages respectively, cultivated in the presence of 20 ng/ml [p24-Gag] R5-tropic HIV-1 primary isolate (93BR029, NIH AIDS Reagents program) for 2 hours. Virus was then removed by thorough washes and fresh complete medium was added to macrophage cultures. Zidovudine (AZT) (NIH AIDS Reagent Program) was added at 10 μM to *ex vivo*-infected tissue macrophages as negative control when quantifying productive infection. Viral production in the days following infection was quantified in culture supernatants by enzyme-linked immunosorbent assays (ELISA) for HIV-1 p24-Gag (p24 Innotest HIV-1 ELISA, InGen, Diaxonhit group, France) for up to 60 days. We defined that viral latency was reached when viral detection in the macrophage culture supernatants become undetectable by the p24 ELISA employed as we described [6]. Integrated HIV DNA was assessed by Alu-gag nested PCR as described [12].

Latency reversal assays. Latently infected macrophages, either infected *in vitro* or selected from urethral tissue of cART-suppressed HIV-infected individuals were treated with 1 μg/ml of bacterial LPS which reactivates viral production[6, 9, 11, 12], and with 5 to 20 μg/ml of purified S100 calcium binding protein A8 (S100A8) [37]. LPS or S100A8 were added to macrophage cultures for 48 hours to reactivate viral production that was then measured in culture supernatants.

In latently infected M4-MDM, p24-Gag ELISA was performed directly on culture supernatants after 48 hours of latency reversal with LPS or S100A8 (5 to 20 μg/ml). Cell fractions were processed for HIV-1 LTR RT-qPCR as described [64]. Reversal of HIV latency was carried out in the presence of 10 μM Zidovudine (AZT) in some experiments.

In tissue macrophages obtained from healthy donors and latently infected *in vitro*, p24-Gag ELISA was performed in the days following infection until HIV-1 production becomes undetectable by this method. Next, the tissue macrophages were reactivated with LPS or S100A8 (10 μg/ml) for 48 hours and the macrophages were processed for HIV-1 LTR RT-qPCR as described [64]. To take into account the variability in the acute HIV-1 infection level of tissue macrophages in different donor samples, the amount of virus produced upon reactivation was expressed by the ratio between the number of HIV-1 LTR copies

found in reactivated macrophages and the maximal cumulative production of p24-Gag detected by ELISA before the latency.

In tissue macrophage reservoirs obtained from cART-suppressed HIV-1-infected individuals and reactivated *ex vivo* with LPS or S100A8 (10 µg/ml), supernatants were collected 48 hours after reactivation. To amplify the small amounts of replication competent virus produced in this case, supernatants were added to $CD4^+$ T-cell lymphoblasts in a viral outgrowth assay, as described below.

Low-level infectious HIV production assessed by viral outgrowth assays. Due to the limited amount of latently infected macrophages generated *in vitro* [24] or obtained *in vivo* [12] and also as the amount of virus released into culture supernatant from latently infected macrophages reactivated *in vitro* is below the limit of detection for most conventional techniques, it was necessary to amplify the reactivated HIV by an outgrowth assays using $CD4^+$ T-cell lymphoblasts [12, 65] .

Accordingly, the production of replication-competent virus following HIV latency reversal of infected macrophages was quantified by an adapted viral outgrowth assay performed as follows: after XX days of latency reversal, supernatants of infected macrophages were incubated with $CD4^+$ T-cell lymphoblasts from healthy donors produced as described [65] for 7 days in RPMI 1640 with 10% FCS supplemented with 10 U/ml IL-2 (Sigma-Aldrich). Lymphoblasts were centrifuged at 300g, 10 min, and resuspended in fresh complete medium containing 10 U/ml IL-2 for additional 7 days. Then, lymphoblasts were centrifuged again and cell pellets were processed for RT-qPCR of HIV-1 long terminal repeat as described [64].

Multiparametric Flow cytometry. Multiparametric flow cytometry was performed as described [12] with simplifications in the gating strategy: our previous experience with urethral tissues [12] allowed us to identify dead cells in FSC/SSC dot plots of tissue cells suspension, gating viable cells (Supplementary Figure 3a-b). Doublets were excluded in an FSC-A/FSC-H dot plot and macrophages were gated in a CD3/CD68 dot plot as $CD68^+CD3^{neg}$ cell population (Supplementary Figure 3b-c). The antibodies used in this study were designed and validated for flow cytometry and are disclosure in Supplementary Table Data 1. Immunofluorescence of labeled tissue cell suspensions was acquired on an LSR II cytometer (BD Biosciences). Fluorescence specificity and compensation were established in the BD CellQuest (BD Biosciences) data acquisition software using BD CompBead Compensation Particles (BD Biosciences) for each fluorescence-coupled antibody used in the panel.

Flow cytometry data were analyzed with FlowJo software (FlowJo version X 10.0.7r2 - FlowJo, LCC). UMAPs were generated by concatenation of $CD68^+$ cell population of 4 cART-treated HIV-infected individuals followed by FlowJo UMAP plugin (S100A8, MMP7, CD206, CD163, IL-1R and IL-4R markers used). Clustering analysis on UMAP was performed by FlowSom plugin to define the different macrophage populations.

The correlation between expression of different markers comparing macrophages from different origins (derived *in vitro* or obtained from urethral tissues) was performed by ClustVis software [66] using the mean percentage of macrophages expressing these markers in a total population of macrophages. The correlation analysis is shown as a heatmap generated using the following parameters: correlation as clustering distance and average as method for clustering between different macrophage samples; tree ordering set as tightest cluster first.

Fluorescence* in situ *hybridization coupled to flow cytometry (FISH-flow). The detection of HIV-infected cells in the tissue cell suspensions was performed by immunostaining of viral protein p24-Gag (anti-p24 clone KC57, FITC), combined with fluorescence *in situ* hybridization using mRNA Cy5-tagged probes covering *gag*, *pol* and *env* HIV genes, both labeling being quantified at the single-cell level by flow cytometry, a technique described as FISH-flow [67]. Probes were designed by Stellaris Probe Designer program (http://www.singlemoleculefish.com) as we described [34] and the probe sets are detailed in Supplementary Table Data 1. FISH-flow recently succeeded in detecting the very low amount of latent HIV-1 reservoir cells in cART-treated patients, which comprises around 1 infected cell per million $CD4^+$ T-cells [35, 67, 68]. The technique was performed here as described [64] and was employed in the context of multiparametric flow cytometry using a similar gating strategy as described above (Supplementary Figure 4c).

Quantification of PF4 expression in tissues. Paraformaldehyde-fixed, paraffin-embedded urethral tissue pieces were sectioned (4µm), deparaffinized in xylene and graded alcohol solutions, treated with Hydrogen Peroxide solution (Advanced Cell Diagnostics, Inc.) for 10 min, heated in boiling RNAscope target retrieval buffer (Advanced Cell Diagnostics, Inc.) for 30 min as recommended by manufacturer for antigen retrieval, incubated with RNAscope Protease Plus (Advanced Cell Diagnostics, Inc.) for 20 min at 40°C, and washed in distilled water. Sections were then blocked for nonspecific staining in a blocking solution (1% w/v BSA, 1% v/v horse serum, 5% v/v human serum, 1% g/v gelatin, and 50 mM EDTA) for 1h at room temperature. Next, sections were labelled with 10 µg/mL CXCL4/PF4 (Chromatec, a-PF4-h1, IgG2b) and 20 µg/mL CD68 (Novus, NB100-683, IgG1) antibody overnight at 4°C. After washing in blocking solution, sections were incubated with 1:200 v/v Cy3-conjugated-anti-mouse-IgG2b (Jackson ImmunoResearch, 115-165-207) and 1:200 v/v Cy5-conjugated-IgG1 (Abcam, ab136127) secondary antibodies for 2h at room temperature. Finally, sections were washed, counterstained with DAPI and mounted with mounting medium (ibidi, 50001). Immunofluorescence was visualised using a Spinning disk unit (Ixplore, Olympus) and analysed using FUJI-image J software [69]. Three scans were taken from each section at ×30 magnification. CXCL4/PF4 positive pixels and area per unit area were calculated as described [70].

Morphological analyses of VCCs. Confocal microscopy after immunostaining was performed as described [6, 12] using anti-CD68 (R&D systems, 10 µg/ml) and anti-p24-Gag antibodies (EVA365 and EVA366, 1:10

v/v each, NIBSC, Center for AIDS Reagents). Acquired z-stacks were reconstructed into three-dimensional image projections in Imaris software (version 9.0.2, Oxford Instruments plc, UK) and visualized using MIP filters. Imaris creates isosurface objects by filtering and segmenting the original data set, attributing dimensional data to these isosurfaces such as volume (μm^3) [71]. The attribution of isosurface objects based on p24-Gag immunostaining in infected macrophages allowed for retrieving volumetric measures of the cluster of p24-Gag signal displayed by these infected cells, corresponding to virus-containing compartments, or VCC [12, 16]. The sum of the volumes measured by all VCCs detected in one cell represents the VCC volume per cell referred in this study, as described [72].

Morphological analyses following* in situ *hybridization. Urethral macrophages were cultivated *ex vivo* in 8-well detachable chamber glass slides (ThermoFisher Scientific) for HIV RNA *in situ* hybridization as described [6, 73], using the RNAscope Multiplex Fluorescent V2 Assay kit (Advanced Cell Diagnostics, Inc.) following manufacturer instructions including treating samples with 30 minutes of boiling Target Retrieval Reagent and 10 minutes at 40°C of Protease Plus before hybridization and amplification steps of the protocol.

For combined detection of HIV RNA and p24-Gag immunostaining, after *in situ* hybridization procedures, samples were treated for 1 hour with a blocking buffer containing 50 mM EDTA, 0.45% cold water fish gelatin (Sigma-Aldrich), 10 mg/ml BSA fraction V (Sigma-Aldrich), 1:100 v/v horse serum and 1:20 v/v human serum in water. Next, samples were incubated overnight at 4°C with 1:1000 v/v of anti-HIV-1 p24-Gag monoclonal antibody (NIH AIDS Reagent Program, catalog number 6457) diluted in blocking buffer. Samples were then incubated with anti-mouse IgG1 secondary antibody coupled to AlexaFluor 488 1:2000 v/v diluted in blocking buffer, washed in PBS and incubated with 10 µM 4′,6-Diamidine-2′-phenylindole dihydrochloride (DAPI) for 15 minutes before coverslips were mounted on slides with anti-fading medium suitable for confocal laser scanning microscopy.

The same protocol was applied to FISH and immunostaining of CD68 and S100A8, using for detection of these markers the following primary and secondary antibodies: anti-human CD68 (R&D MAB20401) and anti-human S100A8/S100A9 heterodimer (R&D MAB45701) both at 10µg/ml, and anti-mouse IgG2b coupled to AlexaFluor 488 (Jackson 115-545-207) or anti-rabbit IgG coupled to Cy5 (Jackson 711-177-003) both at 1:200 v/v.

The complete list of antibodies used in this study is found in Supplementary Table Data 2.

Evaluation of macrophage glycolytic metabolism. Extracellular acidification rate (ECAR) and oxygen consumption rate (OCR) were measured using the XFe96 Analyzer (Agilent Technologies) as described by the manufacturer.

To compare the metabolism of M4- and M2-macrophages, macrophages were preincubated with Seahorse XF DMEM medium pH 7.4 (Agilent) supplemented with 2 mM glutamine (Glucose-free Seahorse medium). The instrument was programmed to sequentially inject compounds into wells of the Seahorse

culture plates in the following order: Glucose (11 mM final well concentration), etomoxir (Sigma-Aldrich) (100 µM final well concentration), 2-deoxyglucose (2-DG) (Sigma-Aldrich) (10mM final well concentration) and electron transport chain inhibitors antimycin A and rotenone (AM/rot)(Agilent) (10 µg/ml each final well concentration). Compounds were diluted in Glucose-free Seahorse medium.

To compare changes in M4-macrophage metabolism upon S100A8 or LPS treatment, macrophages were preincubated with Seahorse XF DMEM medium pH 7.4 (Agilent) supplemented with 2 mM glutamine and 11 mM glucose (complete Seahorse medium). The instrument was programmed to sequentially inject: first, the Seahorse medium alone, LPS (1 µg/ml final well concentration) or S100A8 (10 µg/ml final well concentration) in Seahorse medium; second, etomoxir (100 µM final well concentration); third 2-DG (10 mM final well concentration) and fourth, AM/rot (each 10 µg/ml final well concentration). Compounds were diluted in complete Seahorse medium.

Data obtained was first analyzed by Agilent Seahorse Wave Desktop software (Agilent Technologies) and normalized to cells numbers per well (quantified by microscopic automatic counting algorithms using Imaris software and DAPI fluorescent staining) and to baseline ECAR/OCR levels (last measure before first injection). ECAR/OCR data is therefore shown as mean percentage after baseline normalization (baseline levels defined as 100%). The glycolytic activity refers to a subtraction of the ECAR peak level after first injection and the minimum ECAR level after 2-DG injection.

Energy maps were generated by plotting these ECAR peak levels against corresponding OCR measures acquired at the same time point. ECAR/OCR baseline levels (last measure before first injection) were normalized to correspond to 100. Arrows indicate the increase in either ECAR or OCR levels between baseline measures (before first injection) and the ECAR peak (after first injection).

Cytokines/Chemokine quantification. Urethral mucosa tissues were processed as described [74] to obtain tissue lysates. The cytokines/chemokines CXCL4/PF4, IL-13, M-CSF, MCP-1/CCL2, TRAIL, RANTES/CCL5, MIP-1α /CCL3, GM-CSF, IL-4, MIP-3α/CCL20 and MCP-4/CCL13 were quantified using the Luminex technology (LXSAHM, R&D) on a Bio-Plex 200 (Bio-Rad) according to the manufacturer's recommendations. IFN-γ was quantified using the Human IFN-γ ELISA Development Kit (Mabtech), according to the manufacturer's instructions. The lower limit of quantification (LLOQ) of each cytokine/chemokine is 2 pg/ml (CCL13/MCP-4 and IFNγ), 3 pg/ml (CCL20/MIP-3α), 4 pg/ml (GM-CSF), 7 pg/ml (CCL5/RANTES), 10 pg/ml (TRAIL and CCL2/MCP-1), 16 pg/ml (IL-4), 100 pg/ml (CXCL4/PF4 and CCL3/MIP-1a) and 140 pg/ml (IL-13 and M-CSF). Correlograms were generated in R using *cor*, *cor_test_mat* and *corrplot* functions.

S100A8/S100A8 heterodimer was measured by Quantikine ELISA kit (DS8900, R&D) according to the manufacturer's recommendations.

Cytokine levels were normalized by the protein amount in tissue lysates (mg/ml), quantified by NanoDrop spectrophotometer (ThermoFisher Scientific) using the program Protein A280.

All data associated with this study are in the paper or supplementary materials. Source data are provided with this paper.

Statistical analysis. The results are represented as means with respective standard errors or boxplots. Boxplots represent minima and maxima as lower and upper whiskers, median as centre of the box, and the interquartile range Q1 and Q3 as lower and upper bounds. Statistical tests were performed by SPSS software (IBM), considering normal (parametric tests, Student's *t*-test or ANOVA with post hoc pairwise comparisons) or non-normal distributions (non-parametric tests, Mann-Whitney or Kruskal–Wallis), and two-sided tests. Significant differences were indicated by asterisks considering *p* values below 0.05. For cytokine correlograms, *cor_test_mat* function was employed with Benjamini & Hochberg (BH) adjustment.

Data availability

All data associated with this study are in the paper or supplementary materials. Source data are provided with this paper.

References

1. Honeycutt JB, *et al*. HIV persistence in tissue macrophages of humanized myeloid-only mice during antiretroviral therapy. *Nat Med* **23**, 638-643 (2017).

2. Stevenson M. Role of myeloid cells in HIV-1-host interplay. *J Neurovirol* **21**, 242-248 (2015).

3. Cassol E, Cassetta L, Rizzi C, Alfano M, Poli G. M1 and M2a polarization of human monocyte-derived macrophages inhibits HIV-1 replication by distinct mechanisms. *J Immunol* **182**, 6237-6246 (2009).

4. Carter CA, Ehrlich LS. Cell biology of HIV-1 infection of macrophages. *Annu Rev Microbiol* **62**, 425-443 (2008).

5. Swingler S, Mann AM, Zhou J, Swingler C, Stevenson M. Apoptotic killing of HIV-1-infected macrophages is subverted by the viral envelope glycoprotein. *PLoS Pathog* **3**, 1281-1290 (2007).

6. Real F, Sennepin A, Ganor Y, Schmitt A, Bomsel M. Live Imaging of HIV-1 Transfer across T Cell Virological Synapse to Epithelial Cells that Promotes Stromal Macrophage Infection. *Cell Rep* **23**, 1794-1805 (2018).

7. Eisele E, Siliciano RF. Redefining the viral reservoirs that prevent HIV-1 eradication. *Immunity* **37**, 377-388 (2012).

8. Poltorak A, *et al*. Defective LPS signaling in C3H/HeJ and C57BL/10ScCr mice: mutations in Tlr4 gene. *Science* **282**, 2085-2088 (1998).

9. Liou LY, Herrmann CH, Rice AP. Transient induction of cyclin T1 during human macrophage differentiation regulates human immunodeficiency virus type 1 Tat transactivation function. *J Virol* **76**, 10579-10587 (2002).

10. Marchant D, Neil SJD, McKnight Á. Human immunodeficiency virus types 1 and 2 have different replication kinetics in human primary macrophage culture. *Journal of General Virology* **87**, 411-418 (2006).

11. Pomerantz RJ, Feinberg MB, Trono D, Baltimore D. Lipopolysaccharide is a potent monocyte/macrophage-specific stimulator of human immunodeficiency virus type 1 expression. *J Exp Med* **172**, 253-261 (1990).

12. Ganor Y*, et al.* HIV-1 reservoirs in urethral macrophages of patients under suppressive antiretroviral therapy. *Nat Microbiol* **4**, 633-644 (2019).

13. Kruize Z, Kootstra NA. The Role of Macrophages in HIV-1 Persistence and Pathogenesis. *Front Microbiol* **10**, 2828 (2019).

14. Wong ME, Jaworowski A, Hearps AC. The HIV Reservoir in Monocytes and Macrophages. *Front Immunol* **10**, 1435 (2019).

15. Graziano F*, et al.* Extracellular ATP induces the rapid release of HIV-1 from virus containing compartments of human macrophages. *Proc Natl Acad Sci U S A* **112**, E3265-3273 (2015).

16. Rodrigues V, Ruffin N, San-Roman M, Benaroch P. Myeloid Cell Interaction with HIV: A Complex Relationship. *Front Immunol* **8**, 1698 (2017).

17. Ganor Y*, et al.* The adult penile urethra is a novel entry site for HIV-1 that preferentially targets resident urethral macrophages. *Mucosal Immunol* **6**, 776-786 (2013).

18. de Sousa JR, Da Costa Vasconcelos PF, Quaresma JAS. Functional aspects, phenotypic heterogeneity, and tissue immune response of macrophages in infectious diseases. *Infect Drug Resist* **12**, 2589-2611 (2019).

19. Chistiakov DA, Bobryshev YV, Orekhov AN. Changes in transcriptome of macrophages in atherosclerosis. *J Cell Mol Med* **19**, 1163-1173 (2015).

20. De Paoli F, Staels B, Chinetti-Gbaguidi G. Macrophage phenotypes and their modulation in atherosclerosis. *Circ J* **78**, 1775-1781 (2014).

21. Domschke G, Gleissner CA. CXCL4-induced macrophages in human atherosclerosis. *Cytokine* **122**, 154141 (2019).

22. Appelberg KS, Wallet MA, Taylor JP, Cash MN, Sleasman JW, Goodenow MM. HIV-1 Infection Primes Macrophages Through STAT Signaling to Promote Enhanced Inflammation and Viral Replication. *AIDS Res Hum Retroviruses* **33**, 690-702 (2017).

23. Caputa G, Castoldi A, Pearce EJ. Metabolic adaptations of tissue-resident immune cells. *Nat Immunol* **20**, 793-801 (2019).

24. Castellano P, Prevedel L, Valdebenito S, Eugenin EA. HIV infection and latency induce a unique metabolic signature in human macrophages. *Sci Rep* **9**, 3941 (2019).

25. Valle-Casuso JC*, et al.* Cellular Metabolism Is a Major Determinant of HIV-1 Reservoir Seeding in CD4(+) T Cells and Offers an Opportunity to Tackle Infection. *Cell Metab* **29**, 611-626 e615 (2019).

26. Gleissner CA. Macrophage Phenotype Modulation by CXCL4 in Atherosclerosis. *Front Physiol* **3**, 1 (2012).

27. Martinez FO, Gordon S. The M1 and M2 paradigm of macrophage activation: time for reassessment. *F1000Prime Rep* **6**, 13 (2014).

28. Gordon S. Alternative activation of macrophages. *Nat Rev Immunol* **3**, 23-35 (2003).

29. Romagnani P*, et al.* CXCR3-mediated opposite effects of CXCL10 and CXCL4 on TH1 or TH2 cytokine production. *J Allergy Clin Immunol* **116**, 1372-1379 (2005).

30. Gleissner CA, Shaked I, Little KM, Ley K. CXC chemokine ligand 4 induces a unique transcriptome in monocyte-derived macrophages. *J Immunol* **184**, 4810-4818 (2010).

31. Scheuerer B, *et al.* The CXC-chemokine platelet factor 4 promotes monocyte survival and induces monocyte differentiation into macrophages. *Blood* **95**, 1158-1166 (2000).

32. Domschke G, Gleissner CA. CXCL4-induced macrophages in human atherosclerosis. *Cytokine*, (2017).

33. Erbel C, *et al.* CXCL4-induced plaque macrophages can be specifically identified by co-expression of MMP7+S100A8+ in vitro and in vivo. *Innate Immun* **21**, 255-265 (2015).

34. Arrigucci R, *et al.* FISH-Flow, a protocol for the concurrent detection of mRNA and protein in single cells using fluorescence in situ hybridization and flow cytometry. *Nat Protoc* **12**, 1245-1260 (2017).

35. Baxter AE, *et al.* Single-Cell Characterization of Viral Translation-Competent Reservoirs in HIV-Infected Individuals. *Cell Host Microbe* **20**, 368-380 (2016).

36. Butera ST. Evaluation of Compounds That Prevent Reactivation of HIV-1 in OM-10.1 Cells. *Methods Mol Med* **24**, 201-206 (2000).

37. Vogl T, *et al.* Autoinhibitory regulation of S100A8/S100A9 alarmin activity locally restricts sterile inflammation. *J Clin Invest*, (2018).

38. Vogl T, *et al.* Mrp8 and Mrp14 are endogenous activators of Toll-like receptor 4, promoting lethal, endotoxin-induced shock. *Nat Med* **13**, 1042-1049 (2007).

39. Ryckman C, Robichaud GA, Roy J, Cantin R, Tremblay MJ, Tessier PA. HIV-1 transcription and virus production are both accentuated by the proinflammatory myeloid-related proteins in human CD4+ T lymphocytes. *J Immunol* **169**, 3307-3313 (2002).

40. Campillo-Gimenez L, *et al.* Neutrophils in antiretroviral therapy-controlled HIV demonstrate hyperactivation associated with a specific IL-17/IL-22 environment. *J Allergy Clin Immunol* **134**, 1142-1152 e1145 (2014).

41. Pandiyan P, *et al.* Mucosal Regulatory T Cells and T Helper 17 Cells in HIV-Associated Immune Activation. *Front Immunol* **7**, 228 (2016).

42. Galvan-Pena S, O'Neill LA. Metabolic reprograming in macrophage polarization. *Front Immunol* **5**, 420 (2014).

43. Bouillaud F, Hammad N, Schwartz L. Warburg Effect, Glutamine, Succinate, Alanine, When Oxygen Matters. *Biology (Basel)* **10**, (2021).

44. Bories GFP, Leitinger N. Macrophage metabolism in atherosclerosis. *FEBS Lett* **591**, 3042-3060 (2017).

45. French MA, King MS, Tschampa JM, da Silva BA, Landay AL. Serum immune activation markers are persistently increased in patients with HIV infection after 6 years of antiretroviral therapy despite suppression of viral replication and reconstitution of CD4+ T cells. *J Infect Dis* **200**, 1212-1215 (2009).

46. Hattab S, *et al.* Soluble biomarkers of immune activation and inflammation in HIV infection: impact of 2 years of effective first-line combination antiretroviral therapy. *HIV Med* **16**, 553-562 (2015).

47. Sieweke MH, Allen JE. Beyond stem cells: self-renewal of differentiated macrophages. *Science* **342**, 1242974 (2013).

48. Deeks SG, Tracy R, Douek DC. Systemic effects of inflammation on health during chronic HIV infection. *Immunity* **39**, 633-645 (2013).

49. Churchill MJ, Deeks SG, Margolis DM, Siliciano RF, Swanstrom R. HIV reservoirs: what, where and how to target them. *Nat Rev Microbiol* **14**, 55-60 (2016).

50. Perkins DJ, Patel MC, Blanco JC, Vogel SN. Epigenetic Mechanisms Governing Innate Inflammatory Responses. *J Interferon Cytokine Res* **36**, 454-461 (2016).

51. Nathan C, Ding A. Nonresolving inflammation. *Cell* **140**, 871-882 (2010).

52. Foell D, Wittkowski H, Vogl T, Roth J. S100 proteins expressed in phagocytes: a novel group of damage-associated molecular pattern molecules. *J Leukoc Biol* **81**, 28-37 (2007).

53. Kawai T, Akira S. Signaling to NF-kappaB by Toll-like receptors. *Trends Mol Med* **13**, 460-469 (2007).

54. Hashemi FB*, et al.* Myeloid-related protein (MRP)-8 from cervico-vaginal secretions activates HIV replication. *AIDS* **15**, 441-449 (2001).

55. Endoh Y, Chung YM, Clark IA, Geczy CL, Hsu K. IL-10-dependent S100A8 gene induction in monocytes/macrophages by double-stranded RNA. *J Immunol* **182**, 2258-2268 (2009).

56. Strasser F, Gowland PL, Ruef C. Elevated serum macrophage inhibitory factor-related protein (MRP) 8/14 levels in advanced HIV infection and during disease exacerbation. *J Acquir Immune Defic Syndr Hum Retrovirol* **16**, 230-238 (1997).

57. Cohn LB, Chomont N, Deeks SG. The Biology of the HIV-1 Latent Reservoir and Implications for Cure Strategies. *Cell Host Microbe* **27**, 519-530 (2020).

58. Russell DG, Huang L, VanderVen BC. Immunometabolism at the interface between macrophages and pathogens. *Nat Rev Immunol* **19**, 291-304 (2019).

59. Koo SJ, Garg NJ. Metabolic programming of macrophage functions and pathogens control. *Redox Biol* **24**, 101198 (2019).

60. Palmer CS, Palchaudhuri R, Albargy H, Abdel-Mohsen M, Crowe SM. Exploiting immune cell metabolic machinery for functional HIV cure and the prevention of inflammaging. *F1000Res* **7**, 125 (2018).

61. Netea MG*, et al.* Trained immunity: A program of innate immune memory in health and disease. *Science* **352**, aaf1098 (2016).

62. Clayton KL*, et al.* Resistance of HIV-infected macrophages to CD8(+) T lymphocyte-mediated killing drives activation of the immune system. *Nat Immunol* **19**, 475-486 (2018).

63. Mantovani A, Sica A, Sozzani S, Allavena P, Vecchi A, Locati M. The chemokine system in diverse forms of macrophage activation and polarization. *Trends Immunol* **25**, 677-686 (2004).

64. Real F*, et al.* Platelets from HIV-infected individuals on antiretroviral drug therapy with poor CD4(+) T cell recovery can harbor replication-competent HIV despite viral suppression. *Sci Transl Med* **12**, (2020).

65. Siliciano JD, Siliciano RF. Enhanced culture assay for detection and quantitation of latently infected, resting CD4+ T-cells carrying replication-competent virus in HIV-1-infected individuals. *Methods Mol Biol* **304**, 3-15 (2005).

66. Metsalu T, Vilo J. ClustVis: a web tool for visualizing clustering of multivariate data using Principal Component Analysis and heatmap. *Nucleic Acids Res* **43**, W566-570 (2015).

67. Baxter AE*, et al.* Multiparametric characterization of rare HIV-infected cells using an RNA-flow FISH technique. *Nat Protoc* **12**, 2029-2049 (2017).

68. Grau-Exposito J*, et al.* A Novel Single-Cell FISH-Flow Assay Identifies Effector Memory CD4+ T cells as a Major Niche for HIV-1 Transcription in HIV-Infected Patients. *MBio* **8**, (2017).

69. Schindelin J*, et al.* Fiji: an open-source platform for biological-image analysis. *Nat Methods* **9**, 676-682 (2012).

70. Yeo L*, et al.* Expression of chemokines CXCL4 and CXCL7 by synovial macrophages defines an early stage of rheumatoid arthritis. *Ann Rheum Dis* **75**, 763-771 (2016).

71. Real F, Mortara RA. The diverse and dynamic nature of Leishmania parasitophorous vacuoles studied by multidimensional imaging. *PLoS Negl Trop Dis* **6**, e1518 (2012).

72. Leymarie O, *et al.* Contribution of the Cytoplasmic Determinants of Vpu to the Expansion of Virus-Containing Compartments in HIV-1-Infected Macrophages. *J Virol* **93**, (2019).

73. Deleage C, *et al.* Defining HIV and SIV Reservoirs in Lymphoid Tissues. *Pathog Immun* **1**, 68-106 (2016).

74. Sennepin A, *et al.* The Human Penis Is a Genuine Immunological Effector Site. *Front Immunol* **8**, 1732 (2017).

Acknowledgements

The authors thank the tissue donors for their kind participation in the study. This study was supported by l'Agence Nationale de Recherches sur le Sida et les Hépatites Virales (ANRS) (AO2015-2-17046) and SIDACTION (15CONV03), and Fondation pour la Recherche Medicale (Equipe FRM: EQU201903007830) funds to MB. FR received post-doctoral fellowship from SIDACTION and ANRS, AZ is a doctoral fellow from the China Scholarship Council (CSC), and AS received a post-doctoral fellowship from ANRS.

Author contributions statement

FR, MB: conceived the experiments; MR and SC: collected the patient samples and provided clinical information; FR, AS and MB: performed and analyzed flow cytometry experiments; FR, AZ, AB, BH and MB performed and analyzed confocal microscopy after immunostaining and *in situ* hybridization; FR, AZ, MB: devised and performed viral outgrowth assays; FR, RA, MLG, MB: set up fluorescence *in situ* hybridization coupled to flow cytometry; JR and TV: provided S100 proteins and FR, JR ,TV and MB analyzed S100A8 experimental results; FR, AZ, CR, AL, FB, MB: devised, performed and analyzed Seahorse Analyzer experiments; FR, and MB: wrote the manuscript.

Competing interested statement

The authors declare no competing interests in conducting this study.

Tables

Individual	Age at tissue sampling	years of HIV diagnostic	years of cART initiation	viral load at sampling	cART regimen[1]
1	30	3	NA	undetectable	NA
2	50	NA	NA	undetectable	NA
3	43	22	NA	undetectable	RTV DRV RAL ETR
4	38	23	NA	undetectable	FTC TDF RTV
5	38	NA	NA	undetectable	NA

6	53	NA	11	undetectable	FTC TDF EVG
7	59	NA	NA	undetectable	FTC TDF EVG
8	51	4	NA	undetectable	3TC DTG ABC
9	34	3	3	undetectable	FTC TDF EVG
10	40	14	11	undetectable	FTC TDF EVG
11	41	NA	NA	undetectable	NA
12	36	NA	NA	undetectable	NA
13	59	13	13	undetectable	DTG RPV
14	26	9	9	undetectable	FTC TDF EFV
15	37	8	NA	undetectable	FTC TDF EFV
16	35	16	9	undetectable	FTC TDF RTV DRV
17	32	2	2	undetectable	NA
18	45	18	18	undetectable	3TC ABC LPV RTV
19	45	4	4	undetectable	FTC TDF RTV DRV
20	47	28	10	undetectable	FTC TDF RPV
21	36	10	2	undetectable	3TC DTG ABC
22	65	4	4	undetectable	NA
23	49	24	22	undetectable	3TC DTG
24	44	15	14	undetectable	FTC TDF RPV
25	51	NA	NA	undetectable	NA

[1]cART includes nucleoside reverse transcriptase inhibitors (3TC, lamivudine; ABC, abacavir; FTC, emtricitabine; TDF, tenofovir), non-nucleoside reverse transcriptase inhibitors (EFV, efavirenz; ETR, etravirine; RPV, rilpivirine), protease inhibitors (ATV, atazanavir; DRV, darunavir; FPV, fosamprenavir; RTV, ritonavir; LPV, lopinavir) and integrase inhibitors (DTG, dolutegravir; EVG, elvitegravir; RAL, raltegravir). NA, not available.

Table 1. Clinical information of HIV-infected cART-suppressed individuals enrolled in this study. Table shows the age, years after HIV positive diagnostic and years under combined antiretroviral therapy (cART) of the individuals at the date of tissue sampling. The viral load of these individuals was tested undetectable at date of sampling (HIV RNA copies/ml of blood below the limit of detection of 40 copies/ml). All individuals were receiving different suppressive cART regimens at sampling, although not all regimens were fully disclosed (not available, NA).

Figure legends

Figure 1. Inflammatory M4-macrophages are enriched in the urethral mucosa of cART-suppressed HIV-1 infected-individuals.

(a) Scheme of the different methods applied to evaluate morphologically and functionally the mucosal macrophage HIV reservoir, from processing 0.5 x 0.5 cm mucosal tissue pieces obtained from individuals that underwent gender reassignment.

(b) CXCL4/PF4, IL-13 and IFN-γ cytokine profile of urethral tissue extracts of healthy donors (grey) and cART-suppressed HIV-infected (cART HIV$^+$) individuals (red). The number of individual samples (n) included in the analysis is shown per group and cytokine tested. Mann-Whitney test performed for pairwise comparisons between the two groups of individuals and per cytokine. Source data provided in Source Data file.

(c) Flow cytometry gating strategy for characterization of M4-macrophage subtype in healthy donors (upper example) and cART-suppressed HIV-infected individuals (lower example). From CD68$^+$ CD3^{neg} events (total MΦ), M4-macrophages are defined as S100A8$^+$MMP-7$^+$ events. Frequencies of total MΦ and M4-macrophages among total MΦ are shown as mean with 95% confidence interval in brackets.

(d) Percentage of total MΦ among the tissue cell suspension (Total MΦ population) and percentage of M4-macrophages among total MΦ population (M4 MΦ in total MΦ) in healthy donors (grey, n=7) and cART-suppressed HIV-infected individuals (red, n=7). Mann-Whitney test between healthy donor and cART HIV$^+$ group. Source data provided in Source Data file.

(e) Frequency in percentage of macrophage polarization markers displayed by total MΦ among the tissue cell suspension (Total MΦ population, left graph) and M4-macrophages (M4-macrophages population, right graph) in healthy donors (grey, n=7) and cART-suppressed HIV-infected individuals (red, n=7). Mann-Whitney test between healthy donor and cART HIV$^+$ group. Source data provided in Source Data file.

Figure 2. HIV-1 mucosal macrophage reservoirs form in inflammatory IL-1R$^+$ M4-macrophages *in vivo* as detected at single-cell level.

(a) Identification of HIV reservoir in macrophages identified by HIV RNA detection using FISH coupled to CD68 immunostaining on paraffin-embedded urethral tissue sections from a cART-treated HIV-infected individual. HIV RNA in red, macrophage marker CD68 in green, nuclei stained with DAPI (blue). Image shows the different fluorescent channels of a macrophage HIV reservoir and a high-magnification inset on the right with these channels merged. Bar=10 μm or 3 μm (inset). Image is representative of two cART-treated HIV-infected individual samples.

(b) Representative flow cytometry gating of HIV RNA$^+$p24-Gag$^+$ events acquired in total urethral MΦ population obtained from a healthy donor (upper) and a cART-suppressed HIV-infected individual (lower). Frequencies of HIV RNA$^+$/p24-Gag$^+$ MΦ among total MΦ are shown as mean with 95% confidence interval in brackets (n=5 healthy donors, n=5 cART HIV-infected individuals).

(c) Percentage of HIV RNA$^+$p24-Gag$^+$ events acquired in total urethral MΦ population obtained from these two groups of individuals (n=5 healthy donors, n=5 cART HIV-infected individuals). Dotted red line indicates limit of detection based on healthy donor controls. Mann-Whitney test. Source data provided in Source Data file.

(d) UMAP built from concatenating $CD68^+$ cell populations of different cART HIV^+ individuals (n=4) after clustering analysis of macrophage populations. HIV^+ macrophages were backgated into the UMAP to identify which macrophage profile harbors HIV in cART-treated individuals.

(e) S100A8 is expressed by HIV reservoir macrophages as shown by colocalization of HIV RNA detected using FISH coupled to CD68 and S100A8 immunostaining on paraffin-embedded urethral tissue sections from two cART-treated HIV-infected individuals (#1 and #2). HIV RNA in red, macrophage marker CD68 in green, S100A8 in magenta, nuclei stained with DAPI (blue). Image shows the different fluorescent channels (separated and merged) of the detected macrophage HIV reservoirs found in the mucosal stroma. A high-magnification inset for the one detected in individual #2 is shown on the right, with fluorescent channels merged. Bar=10 μm or 3 μm (inset).

Figure 3. M4-MDM and tissue macrophages from healthy donors infected *in vitro/ex vivo* are surrogates of HIV-1 mucosal macrophage reservoirs.

(a) Hierarchical clustering heatmap of macrophage polarization markers and different macrophage subtypes (obtained *in vivo* or *in vitro*-derived by different stimuli). The intensity of the red color boxes refers to correlation z-scores. Data were obtained from four independent experiments. Source data provided in Source Data file.

(b) Cumulative viral production assessed in *in vitro*-derived MΦ culture supernatants at different days after infection. M2-MDM in blue, non-polarized GM-CSF/M-CSF-derived MDM in grey and M4-MDM in red. Data refers to one experiment representative of three independent experiments. Source data provided in Source Data file.

(c-d) Confocal microscope images of M4-MDM latently infected *in vitro* (34 days post-infection) (n=3) (c) and infected tissue macrophage obtained from cART-suppressed HIV-infected individuals (n=2) (d), immunolabeled for p24-Gag (green) and CD68 (red). Nuclei were stained with DAPI. Merged images are shown as xy projections (main images) and xz/yz projections (framed VCC *a*, VCC *b* and VCC *c* in C right insets, and in D, lower right insets). In D, VCCs framed and magnified in the upper-right inset showing p24-Gag^+ fluorescence signal only. Bar= 1, 5, or 10 μm.

(e-f) Volumetric morphometry of VCCs in infected macrophages obtained from M4-MDM latently infected *in vitro* (n=3) (E) or cART-suppressed HIV-infected tissues (n=2 individuals) (f) after image segmentation in VCC isosurfaces. Dot-plots show the volumes (μm3) of each VCC isosurface detected in different macrophages (identified by number #) obtained from different donors (identified by donor number #). Boxplots represent the sum of VCC volumes per macrophage. Upper panels show VCC isosurfaces (in green, 3D rendering) segmented from the confocal images of infected macrophages. Source data provided in Source Data file.

(g) Cumulative viral production assessed in the supernatants of tissue macrophages obtained from healthy donors (discriminated by different colors, n=4) and infected *ex vivo* at different days after infection. Source data provided in Source Data file.

(h) Cumulative viral production measured in the supernatants of *ex vivo* infected urethral macrophages (pool of three healthy donors) in the absence or presence of 10 μM AZT. Source data provided in Source Data file.

Figure 4. S100A8 reactivate the production of replication-competent virus from tissue macrophage reservoirs.

(a) Quantification of S100A8 monomers and S100A8/S100A9 heterodimers in urethral tissue extracts of healthy donors (grey, n=9) and cART-suppressed HIV-infected individuals (cART HIV^+) (red, n=6). Mann-Whitney test between healthy donor and cART HIV^+ group. Source data provided in Source Data file.

(b) S100A8 cellular expression quantified by flow cytometry of urethral cell suspensions expressed as percentage of $S100A8^+$ cells among the entire tissue cell population and among $CD68^+$ MΦ, or as S100A8 Mean Fluorescence Intensity (MFI) in $S100A8^+$ cells detected among the entire tissue cell population, among $CD68^+$MΦ, or among M4 MΦ. Mann-Whitney test between healthy donor (n=5) and cART HIV^+ group (n=7). Source data provided in Source Data file.

(c) Viral production quantified in M4-MDM culture supernatants after latent infection followed by 2 days of latency reversal induced by indicated S100A8 concentrations or 1 μg/ml LPS. Non-reactivated controls refer to untreated M4-MDM latently infected macrophages. Mann-Whitney test between non-reactivated (untreated) and treated groups pairwise. Data were obtained from five independent experiments. Source data provided in Source Data file.

(d) HIV-1 latency reversal of tissue macrophages obtained from healthy donors latently infected *ex vivo* (n=3), expressed as ratio between macrophage-associated HIV-LTR RNA copies per MΦ and the peak cumulative viral production per MΦ before latency, after 2 days of S100A8 or LPS treatment. Non-reactivated controls refer to ratio from untreated latently infected tissue macrophages. Mann-Whitney test between non-reactivated (untreated) and treated groups pairwise. Source data provided in Source Data file.

(e) Outgrowth of replicating virus produced by tissue macrophage reservoirs obtained from cART-suppressed HIV-infected individuals after S100A8- or LPS-induced latency reversal, expressed as HIV LTR RNA copies per million $CD4^+$ T-cell lymphoblasts from the outgrowth assays. Non-reactivated controls refer to untreated tissue macrophage reservoirs. Pairwise Mann-Whitney test between non-reactivated (untreated, n=5) and treated groups (S100A8, n=5; LPS, n=4). Source data provided in Source Data file.

Figure 5. S100A8-mediated reactivation of HIV macrophage reservoirs depends on a glycolytic metabolic shift.

(a) Extracellular Acidification (ECAR) and Oxygen Consumption Rate (OCR) of M2-MDM (grey) or M4-MDM (red) cultures measured after sequential addition of Seahorse medium with glucose, etomoxir (eto), 2-deoxyglucose (2-DG) and antimycin/rotenone (AM/rot). Results are shown as mean percentages (+/- SEM) of

rate increase/decrease from baseline rate (time point before glucose injection) for each technical replicate. Data obtained from n=4 independent experiments. Source data provided in Source Data file.
(b) Glycolytic activity of M2-MDM (grey) or M4-MDM (red) groups, which refers to the maximum ECAR reached after glucose injection deduced from the minimum ECAR reached after 2-DG injection. Mann-Whitney test. Data obtained from n=4 independent experiments. Source data provided in Source Data file.
(c) ECAR and OCR measured in M4-MDM cultures non-stimulated (medium with glucose) or stimulated with S100A8 or LPS in the presence of glucose, followed by sequential injection of etomoxir (eto), 2-deoxyglucose (2-DG) and antimycin/rotenone (AM/rot). Results are displayed as mean percentages (+/- SEM) of rate increase/decrease from baseline rate (time point before glucose injection) for each technical replicate. Data obtained from n=4 independent experiments. Source data provided in Source Data file.
(d) Glycolytic activity of non-stimulated and S100A8- or LPS-stimulated M4-MDM. ANOVA with Bonferroni post hoc test. Data obtained from n=4 independent experiments. Source data provided in Source Data file.
(e-f) Outgrowth of replicating virus produced by tissue macrophage reservoirs obtained from cART-suppressed HIV-infected individuals after S100A8 latency reversal with or without 2-DG pre-treatment. (e) Scheme of the experiment measuring the reactivation of macrophage HIV reservoirs obtained *in vivo* from urethral tissues *ex vivo* using the different stimuli, namely S100A8, S100A8 preceded by a 2-DG pre-treatment, and LPS. The supernatants of reactivated macrophages were added to $CD4^+$T-cells in an outgrowth assay which readout is the detection of HIV RNA in the $CD4^+$T-cells by qPCR. (f) Outgrowth of virus produced by reactivated macrophage HIV reservoirs expressed as cell-associated HIV LTR RNA copies per million $CD4^+$ T-cell lymphoblasts employed in outgrowth assays. Non-reactivated controls refer to untreated tissue macrophage reservoirs. ANOVA with Bonferroni correction. Data were obtained from three different cART HIV-infected individuals. Source data provided in Source Data file.

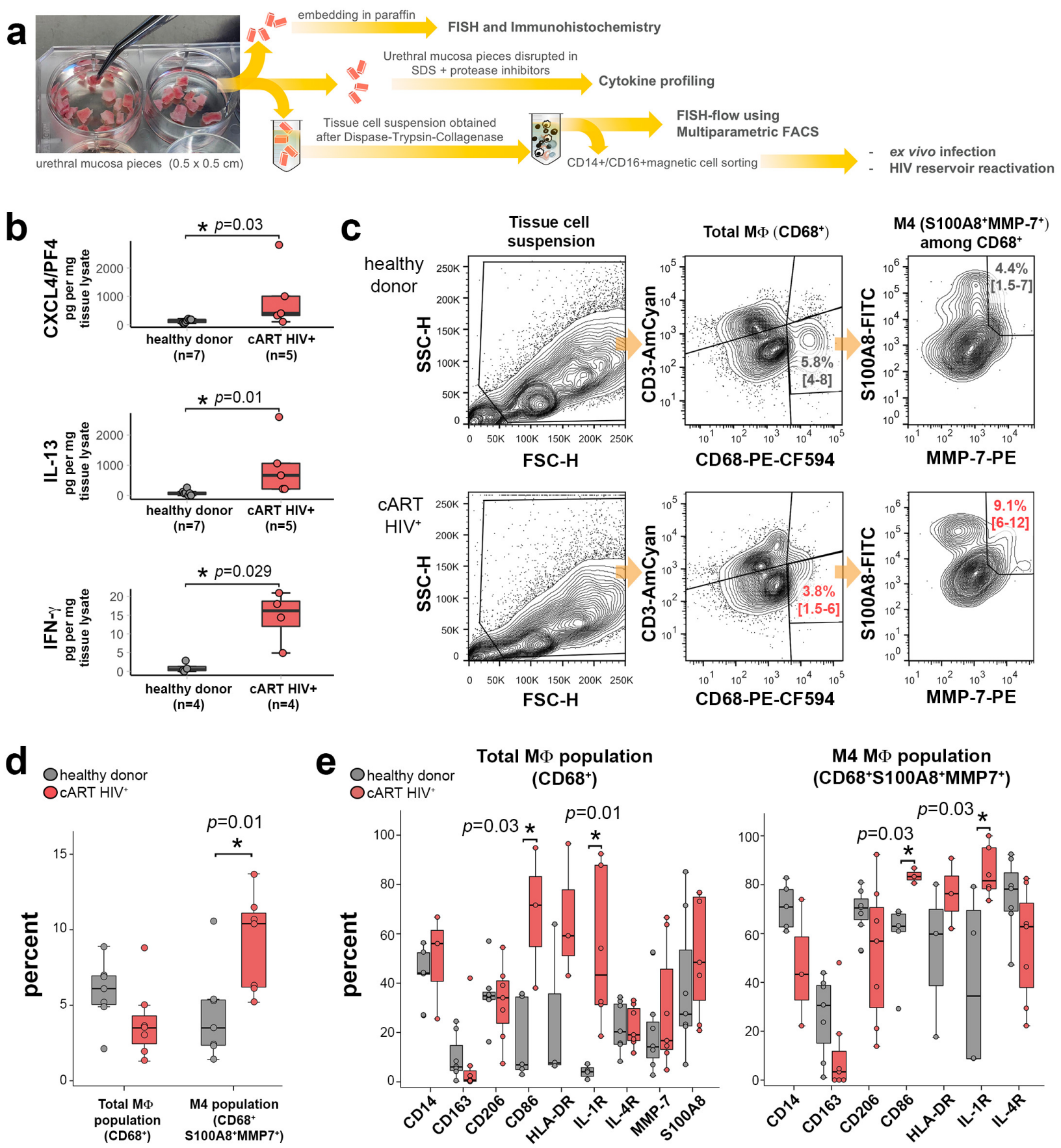
a
urethral mucosa pieces (0.5 x 0.5 cm)
embedding in paraffin
FISH and Immunohistochemistry
Urethral mucosa pieces disrupted in SDS + protease inhibitors
Cytokine profiling
Tissue cell suspension obtained after Dispase-Trypsin-Collagenase
FISH-flow using Multiparametric FACS
CD14+/CD16+magnetic cell sorting
- ex vivo infection
- HIV reservoir reactivation
b
CXCL4/PF4 pg per mg tissue lysate
* p=0.03
healthy donor (n=7)
cART HIV+ (n=5)
IL-13 pg per mg tissue lysate
* p=0.01
healthy donor (n=7)
cART HIV+ (n=5)
IFN-γ pg per mg tissue lysate
* p=0.029
healthy donor (n=4)
cART HIV+ (n=4)
c
Tissue cell suspension
Total MΦ (CD68+)
M4 (S100A8+MMP-7+) among CD68+
healthy donor
cART HIV+
SSC-H
FSC-H
CD3-AmCyan
CD68-PE-CF594
S100A8-FITC
MMP-7-PE
4.4% [1.5-7]
5.8% [4-8]
9.1% [6-12]
3.8% [1.5-6]
d
healthy donor
cART HIV+
percent
p=0.01
*
Total MΦ population (CD68+)
M4 population (CD68+ S100A8+MMP7+)
e
healthy donor
cART HIV+
Total MΦ population (CD68+)
M4 MΦ population (CD68+S100A8+MMP7+)
percent
p=0.03
*
p=0.01
*
CD14
CD163
CD206
CD86
HLA-DR
IL-1R
IL-4R
MMP-7
S100A8

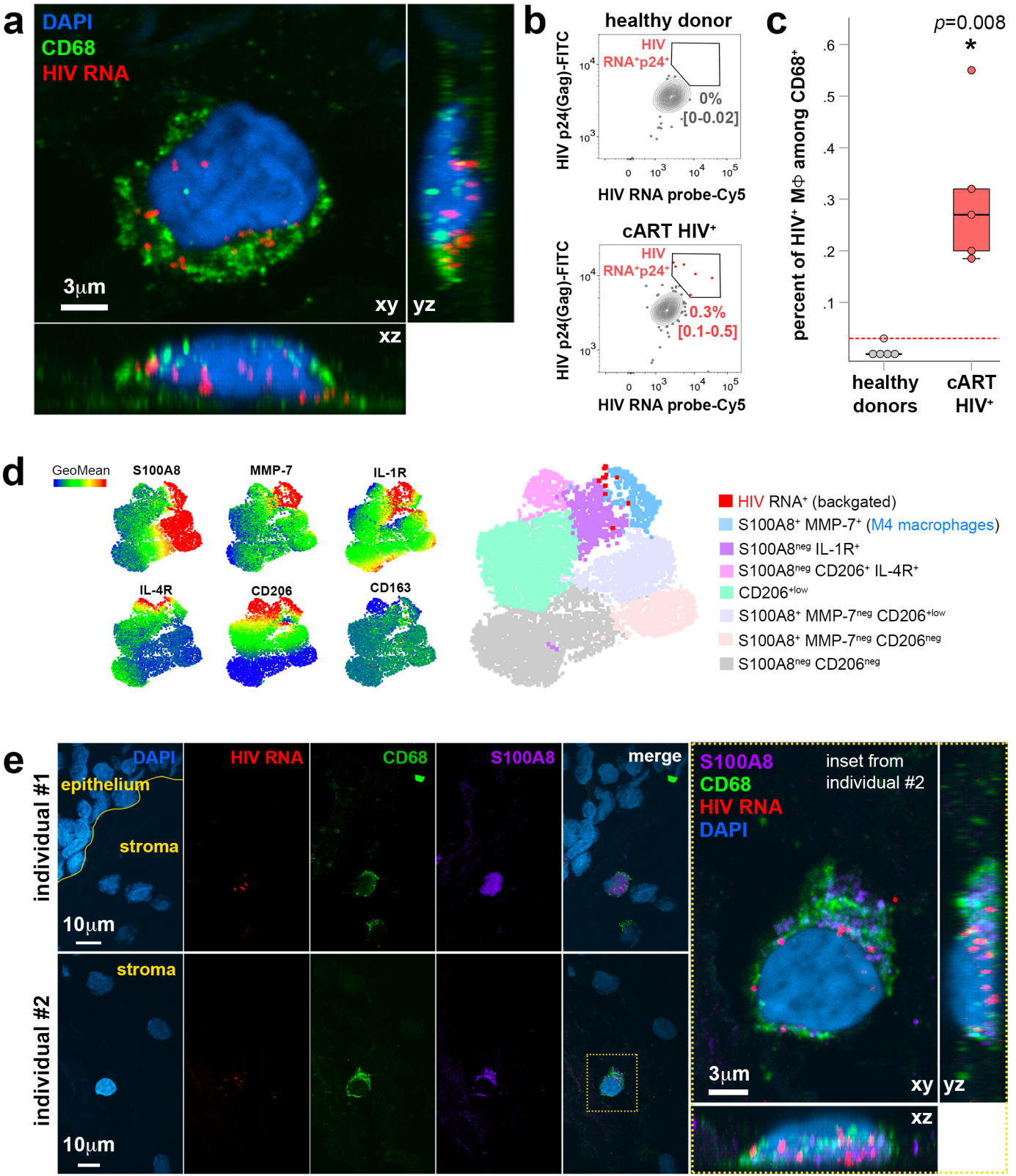
a
DAPI
CD68
HIV RNA
3μm
xy
yz
xz
b
healthy donor
HIV RNA+p24+
0%
[0-0.02]
HIV p24(Gag)-FITC
HIV RNA probe-Cy5
cART HIV+
HIV RNA+p24+
0.3%
[0.1-0.5]
HIV p24(Gag)-FITC
HIV RNA probe-Cy5
c
p=0.008
*
percent of HIV+ MΦ among CD68+
.6
.5
.4
.3
.2
.1
healthy donors
cART HIV+
d
GeoMean
S100A8
MMP-7
IL-1R
IL-4R
CD206
CD163
HIV RNA+ (backgated)
S100A8+ MMP-7+ (M4 macrophages)
S100A8neg IL-1R+
S100A8neg CD206+ IL-4R+
CD206+low
S100A8+ MMP-7neg CD206+low
S100A8+ MMP-7neg CD206neg
S100A8neg CD206neg
e
individual #1
individual #2
DAPI
epithelium
stroma
10μm
HIV RNA
CD68
S100A8
merge
S100A8
CD68
HIV RNA
DAPI
inset from individual #2
3μm
xy
yz
xz

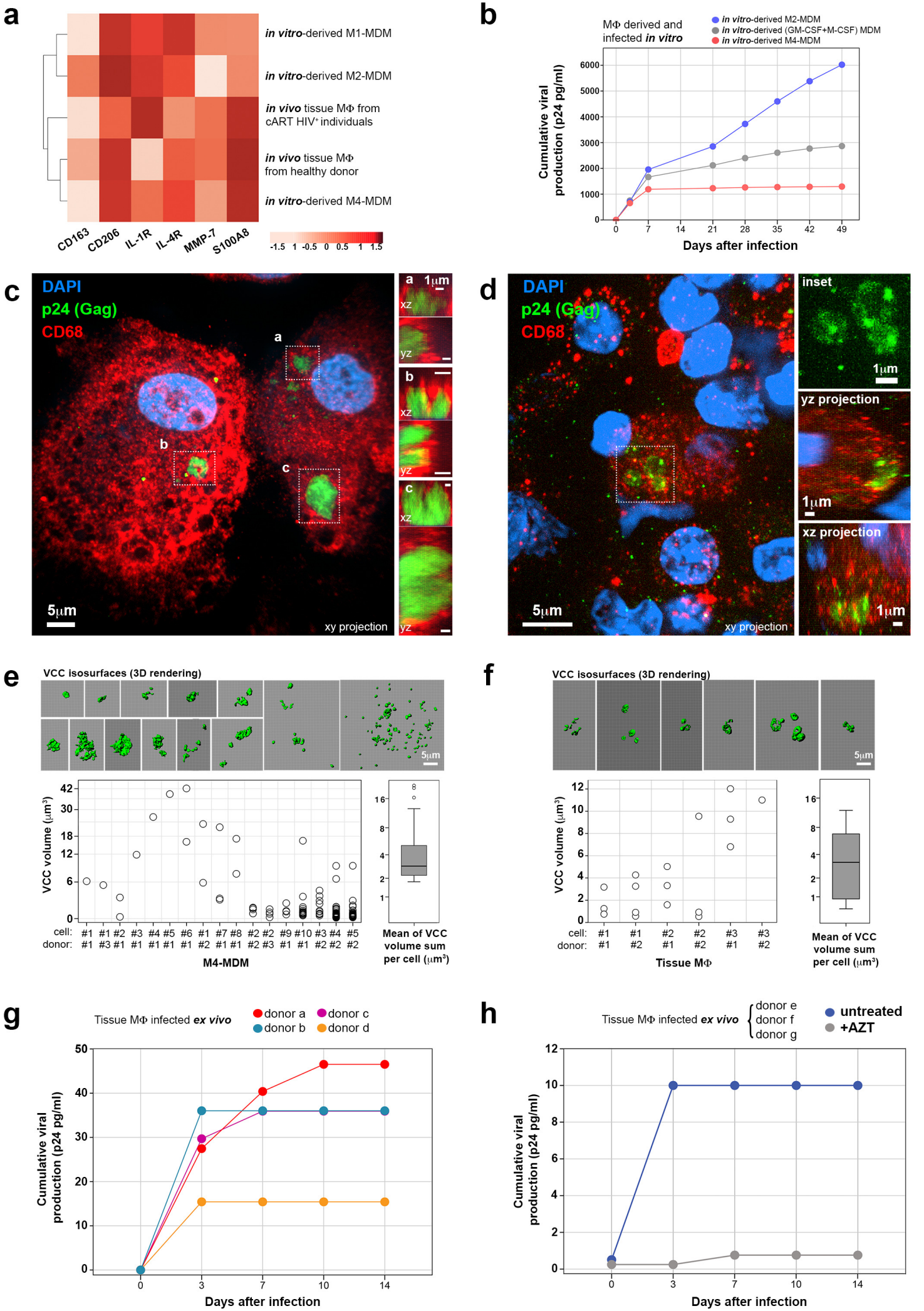
a
in vitro-derived M1-MDM
in vitro-derived M2-MDM
in vivo tissue MΦ from cART HIV+ individuals
in vivo tissue MΦ from healthy donor
in vitro-derived M4-MDM
CD163
CD206
IL-1R
IL-4R
MMP-7
S100A8
-1.5 1 -0.5 0 0.5 1 1.5
b
MΦ derived and infected in vitro
in vitro-derived M2-MDM
in vitro-derived (GM-CSF+M-CSF) MDM
in vitro-derived M4-MDM
Cumulative viral production (p24 pg/ml)
Days after infection
c
DAPI
p24 (Gag)
CD68
xy projection
5μm
1μm
xz
yz
d
DAPI
p24 (Gag)
CD68
inset
yz projection
xz projection
xy projection
e
VCC isosurfaces (3D rendering)
VCC volume (μm³)
cell:
donor:
M4-MDM
Mean of VCC volume sum per cell (μm³)
f
VCC isosurfaces (3D rendering)
Tissue MΦ
g
Tissue MΦ infected ex vivo
donor a
donor b
donor c
donor d
h
Tissue MΦ infected ex vivo
donor e
donor f
donor g
untreated
+AZT

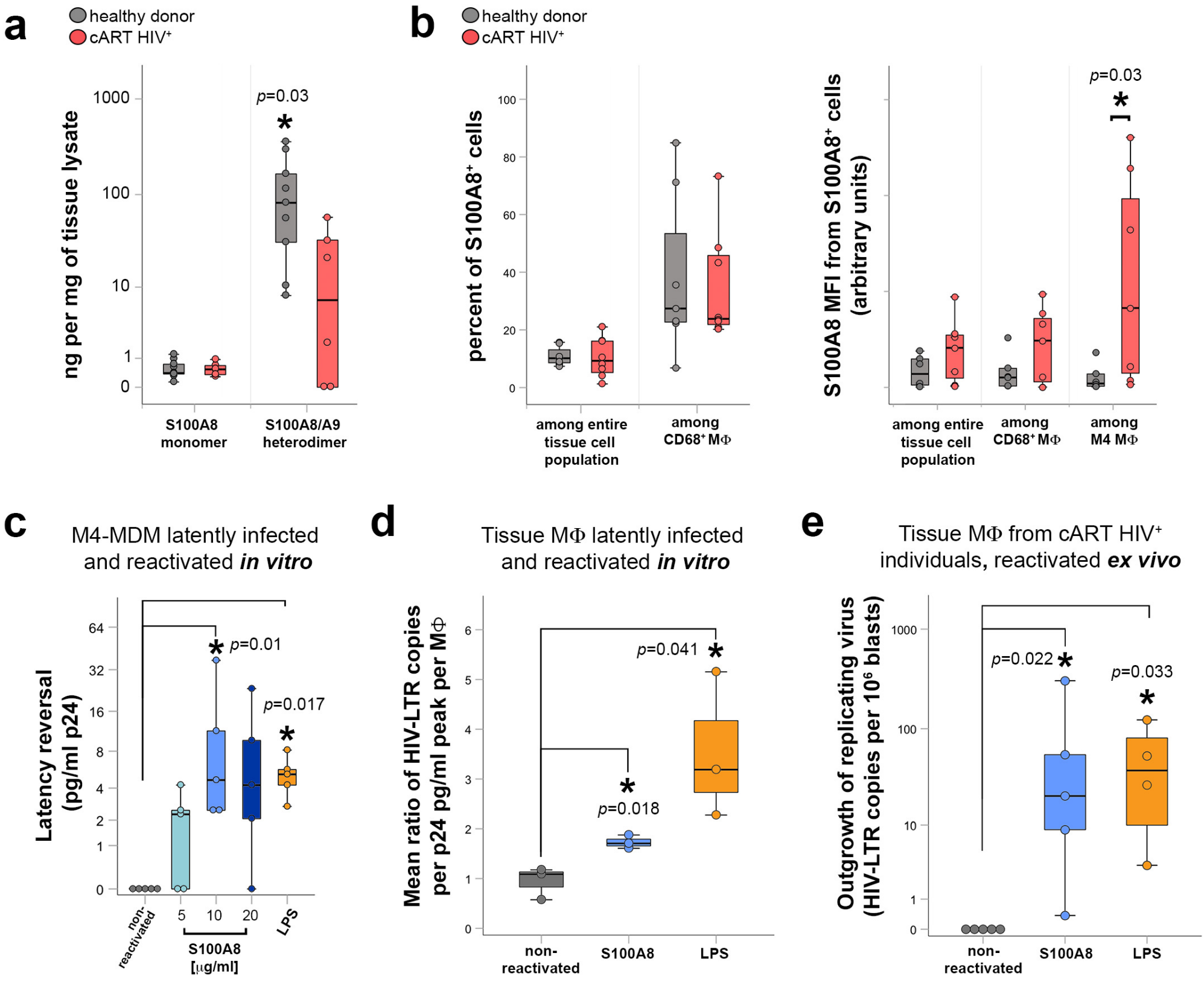
a
healthy donor
cART HIV+
ng per mg of tissue lysate
1000
100
10
1
0
p=0.03
*
S100A8 monomer
S100A8/A9 heterodimer
b
healthy donor
cART HIV+
percent of S100A8+ cells
100
80
60
40
20
0
among entire tissue cell population
among CD68+ MΦ
S100A8 MFI from S100A8+ cells (arbitrary units)
p=0.03
*
among entire tissue cell population
among CD68+ MΦ
among M4 MΦ
c
M4-MDM latently infected and reactivated in vitro
Latency reversal (pg/ml p24)
64
32
16
8
4
2
1
0
p=0.01
*
p=0.017
*
non-reactivated
5
10
20
LPS
S100A8 [μg/ml]
d
Tissue MΦ latently infected and reactivated in vitro
Mean ratio of HIV-LTR copies per p24 pg/ml peak per MΦ
6
5
4
3
2
1
0
p=0.041
*
*
p=0.018
non-reactivated
S100A8
LPS
e
Tissue MΦ from cART HIV+ individuals, reactivated ex vivo
Outgrowth of replicating virus (HIV-LTR copies per 10^6 blasts)
1000
100
10
1
0
p=0.022
*
p=0.033
*
non-reactivated
S100A8
LPS

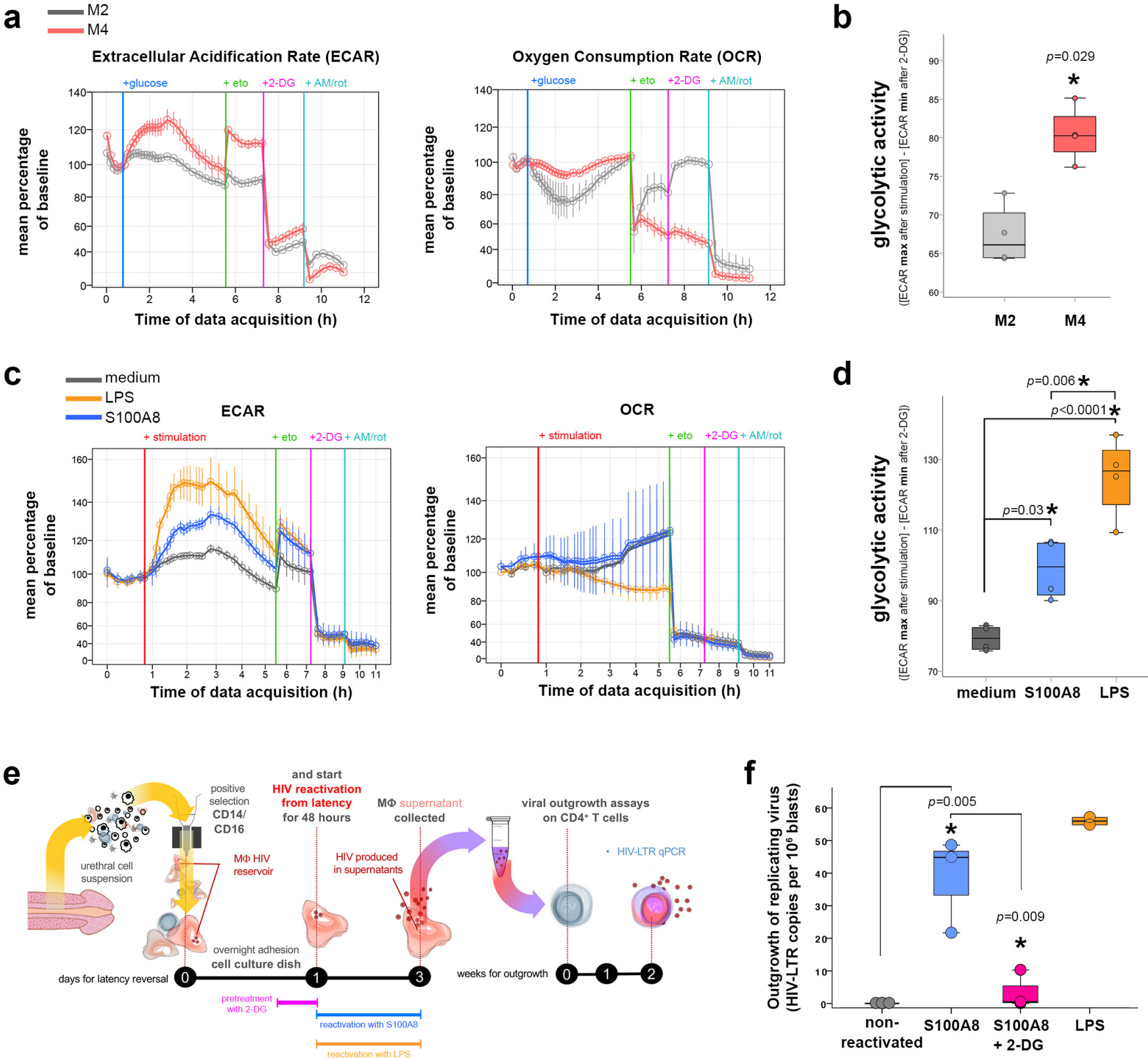
a
M2
M4
Extracellular Acidification Rate (ECAR)
Oxygen Consumption Rate (OCR)
+glucose
+ eto
+2-DG
+ AM/rot
mean percentage of baseline
Time of data acquisition (h)
b
glycolytic activity
([ECAR max after stimulation] - [ECAR min after 2-DG])
p=0.029
M2
M4
c
medium
LPS
S100A8
ECAR
OCR
+ stimulation
d
p=0.006
p<0.0001
p=0.03
medium
S100A8
LPS
e
positive selection CD14/ CD16
urethral cell suspension
MΦ HIV reservoir
overnight adhesion cell culture dish
and start HIV reactivation from latency for 48 hours
MΦ supernatant collected
HIV produced in supernatants
viral outgrowth assays on CD4+ T cells
HIV-LTR qPCR
days for latency reversal
weeks for outgrowth
pretreatment with 2-DG
reactivation with S100A8
reactivation with LPS
f
Outgrowth of replicating virus (HIV-LTR copies per 10⁶ blasts)
p=0.005
p=0.009
non-reactivated
S100A8
S100A8 + 2-DG
LPS